OXFORD

Human Molecular Genetics, 2017, Vol. 26, No. 5 843–859

doi: 10.1093/hmg/ddx001
Advance Access Publication Date: 5 January 2017
Original Article

ORIGINAL ARTICLE

Cyclodextrin has conflicting actions on autophagy flux *in vivo* in brains of normal and Alzheimer model mice

Dun-Sheng Yang[1,2,*], Philip Stavrides[1], Asok Kumar[1,2], Ying Jiang[1,2], Panaiyur S. Mohan[1,2], Masuo Ohno[1,2], Kostantin Dobrenis[3], Cristin D. Davidson[3], Mitsuo Saito[1,2], Monika Pawlik[1], Chunfeng Huo[1], Steven U. Walkley[3] and Ralph A. Nixon[1,2,4,*]

[1]Nathan Kline Institute, Orangeburg, NY, USA, [2]Department of Psychiatry, New York University Langone Medical Center, New York, NY, USA, [3]Dominick P. Purpura Department of Neuroscience, Albert Einstein College of Medicine, Bronx, NY, USA and [4]Cell Biology, New York University Langone Medical Center, New York, NY, USA

*To whom correspondence should be addressed at: Nathan S. Kline Institute, 140 Old Orangeburg Road, Orangeburg, NY 10962, USA. Tel: +1 8453982173; Fax: +1 8453985422; Email: dyang@nki.rfmh.org (D.-S.Y.); Tel: +1 8453985423; Fax: +1 8453985422; Email: nixon@nki.rfmh.org (R.A.N.)

Abstract

2-hydroxypropyl-β-cyclodextrin (CYCLO), a modifier of cholesterol efflux from cellular membrane and endo-lysosomal compartments, reduces lysosomal lipid accumulations and has therapeutic effects in animal models of Niemann-Pick disease type C and several other neurodegenerative states. Here, we investigated CYCLO effects on autophagy in wild-type mice and TgCRND8 mice—an Alzheimer's Disease (AD) model exhibiting β-amyloidosis, neuronal autophagy deficits leading to protein and lipid accumulation within greatly enlarged autolysosomes. A 14-day intracerebroventricular administration of CYCLO to 8-month-old TgCRND8 mice that exhibit moderately advanced neuropathology markedly diminished the sizes of enlarged autolysosomes and lowered their content of GM2 ganglioside and Aβ-immunoreactivity without detectably altering amyloid precursor protein processing or extracellular Aβ/β-amyloid burden. We identified two major actions of CYCLO on autophagy underlying amelioration of lysosomal pathology. First, CYCLO stimulated lysosomal proteolytic activity by increasing cathepsin D activity, levels of cathepsins B and D and two proteins known to interact with cathepsin D, NPC1 and ABCA1. Second, CYCLO impeded autophagosome-lysosome fusion as evidenced by the accumulation of LC3, SQSTM1/p62, and ubiquitinated substrates in an expanded population of autophagosomes in the absence of greater autophagy induction. By slowing substrate delivery to lysosomes, autophagosome maturational delay, as further confirmed by our *in vitro* studies, may relieve lysosomal stress due to accumulated substrates. These findings provide *in vivo* evidence for lysosomal enhancing properties of CYCLO, but caution that prolonged interference with cellular membrane fusion/autophagosome maturation could have unfavorable consequences, which might require careful optimization of dosage and dosing schedules.

Introduction

Cyclodextrins are cyclic oligomers of glucose with a relatively hydrophilic exterior surface and a hydrophobic interior cavity making them useful in medication formulations to improve the solubility, stability and bioavailability of poorly water-soluble drugs (1,2). Cyclodextrins, including the β-cyclodextrin derivative 2-hydroxypropyl-β-cyclodextrin (CYCLO or HP-β-CD), have attracted additional interest as reagents that can modulate

Received: August 24, 2016. **Revised:** November 29, 2016. **Accepted:** January 3, 2016

cholesterol efflux from cellular membrane and endo-lysosomal compartments and have ameliorative effects in animal models of disease states where cholesterol metabolism is central to pathogenesis, including Niemann-Pick type C (NPC) and, more recently, atherosclerosis (3).

In NPC, mutations in *NPC1* or *NPC2* genes cause cholesterol mistrafficking and massive lipid storage in endo-lysosomal compartments, which lead to profoundly impaired neurodevelopment, neurodegeneration, and premature death (4–6). CYCLO administration in mouse and cat models of NPC has been shown recently to decrease the massive lipid storage, delay neurodegeneration, and increase lifespan substantially (7–14). Clinical trials of CYCLO in NPC are currently underway (15–18). A possible mechanism of action suggested by *in vitro* studies in NPC cells is that CYCLO trafficked to lysosomes via endocytosis shuttles cholesterol to exit sites on the lysosomal membrane. This action largely bypasses the need for NPC1 and NPC2, two endo-lysosomal proteins acting cooperatively to mediate cholesterol efflux from late endosomes-lysosomes and secondarily facilitate metabolism of other lipids (19–23).

Although they are distinctly different neurological disorders, NPC and Alzheimer's Disease (AD) exhibit notable neuropathological similarities (24,25), including abundant neurofibrillary tangles (tauopathy) (26,27), varying degrees of β-amyloid deposition (28,29), AD-related enlargement of endosomes (29,30), endo-lysosomal lipid storage and impaired proteolysis (31–34), and hallmark neuritic dystrophy characterized by grossly swollen neurites containing mainly autophagic vacuoles (32,35). There is also strong evidence that AD pathogenesis, like NPC, involves abnormalities in the metabolism/catabolism of cholesterol and other lipids (36,37).

We have previously reported that the TgCRND8 mouse model of AD, expressing human amyloid precursor protein (APP) with the Swedish (K670N/M671L) and Indiana (V717F) mutations and aggressively developing amyloid pathology (38), also features impaired lysosomal proteolytic function and lysosomal pathology characterized by the giant autolysosomes containing accumulated incompletely digested substrates, including Aβ-immunoreactive material and lipids such as GM2 and GM3 (31,39). This model is therefore ideal for testing therapeutic agents with potential for targeting the autophagic-lysosomal system, lipid metabolism and/or amyloid pathology (including intracellular Aβ/APP CTFs). In this study, we investigated whether or not short-term treatment with CYCLO in adult TgCRND8 could reverse the well-developed neuropathology present in mice at this age, as an earlier study had shown that chronic peripheral CYCLO administration (s.c. injections) for months prior to disease onset had significant therapeutic effects in an AD mouse model (40). In light of persistent questions about CYCLO penetration across the blood brain barrier, we administered CYCLO intracranially [intracerebroventricular (ICV) infusion or intrahippocampal injection]. We focused on the *in vivo* actions of CYCLO on autophagy, which are largely unknown even though the effects of cyclodextrins on autophagy *in vitro* have been reported (33,41–44).

Results

Short-term intracranial administration of CYCLO ameliorates intraneuronal pathology in TgCRND8 mice

TgCRND8 mice accumulate intraneuronal giant autolysosomes (usually > 1.5 μm and up to 5 or 6 μm depending on ages, in diameter) containing Aβ/APP metabolites (39) and abnormal amounts of incompletely digested lipids and proteins (31). To examine the effects of CYCLO on autophagy, we first probed brain sections of TgCRND8 with an anti-CTSD/cathepsin D antibody to detect lysosomal compartments. CYCLO-treated brains (ICV infusion) (Fig. 1A2 and A5) exhibited reduced numbers of giant autolysosomes in the CA1 sector (Fig. 1A3, left) compared to those from saline-infused brains (Fig. 1A1 and A4). Conversely, smaller CTSD-positive autolysosomes/lysosomes increased commensurately in TgCRND8 brain, yielding comparable total numbers of CTSD-positive granules under both conditions (Fig. 1A3, left) and suggesting that CYCLO reduced the size of giant autolysosomes, which was further supported by calculations of total autolysosomal/lysosomal volumes showing a decreased volume after CYCLO treatment (Fig. 1A3, right).

To examine the effect of CYCLO on the marked lipid accumulation in lysosome-related compartments previously reported in TgCRND8 brain (31), we examined ganglioside GM2 immunoreactivity as an indicator of lipid accumulation. CYCLO treatment reduced the number of GM2-positive granules (Fig. 1B1–B3), similar to its effect in NPC-deficient mice (9). Moreover, the CYCLO ICV infusion for 14 days also lowered 4G8 immunoreactivity, which is located within lysosomal compartments as revealed previously by double labeling of 4G8 with a lysosomal marker CTSD (39), reflecting clearance of intraneuronal amyloidogenic peptides. As shown in Figure 1C, the numerous 4G8-positive large granules (> 1.5 μm in diameter) seen in the hippocampal CA1 sector of saline-treated TgCRND8 mice (Fig. 1C1) declined concomitantly with CYCLO treatment (Fig. 1C2–C3).

To further confirm these effects of CYCLO, we injected CYCLO directly into the hippocampus (Table 1) of TgCRND8 mice that were then sacrificed after 7 days and coronal brain sections were immunostained with a CTSD antibody (Fig. 1D). Compared to the CA1 sector on the saline-injected side of the brain (Fig. 1D1), the CYCLO-injected side (Fig. 1D2) displayed clearly reduced numbers of giant autolysosomes (i.e. > 1.5 μm in diameter, Fig. 1D3). Cresyl violet staining of the same sections (not shown) revealed no nuclear condensation or loss, which excluded the possibility that these effects were due to cell loss or degeneration induced by CYCLO. Collectively, these findings indicate that CYCLO has actions on the autophagic pathway *in vivo*, consistent with *in vitro* studies (33,41–45).

Short-term ICV administration of CYCLO does not affect autophagy induction

To identify which stage(s) in the autophagy pathway may be responsible for the CYCLO-induced ameliorative effects shown in Figure 1, we first analyzed a range of protein markers for autophagy induction in brain homogenates from CYCLO- or saline-infused TgCRND8 or WT mice (Fig. 2). Contrary to earlier *in vitro* findings in human fibroblasts (42), we did not detect changes in the markers of MTOR-dependent autophagy induction (e.g. total and phosphor-MTOR, total and phosphor-RPS6KB1/p70S6 kinase) in samples from CYCLO-infused mice (Fig. 2).

As for the MTOR-independent autophagy pathways (46), we assessed if CAPN/calpain was activated by examining the levels of one of its substrates, α-spectrin. Similar levels of full-length α-spectrin (270 kDa) were detected in CYCLO- or saline-infused samples, while CAPN-cleaved α-spectrin fragments (expected at 150 kDa) were hardly detectable (Fig. 2). Given that CAPN, if activated, can inhibit autophagy by cleaving ATG5 (47,48), we

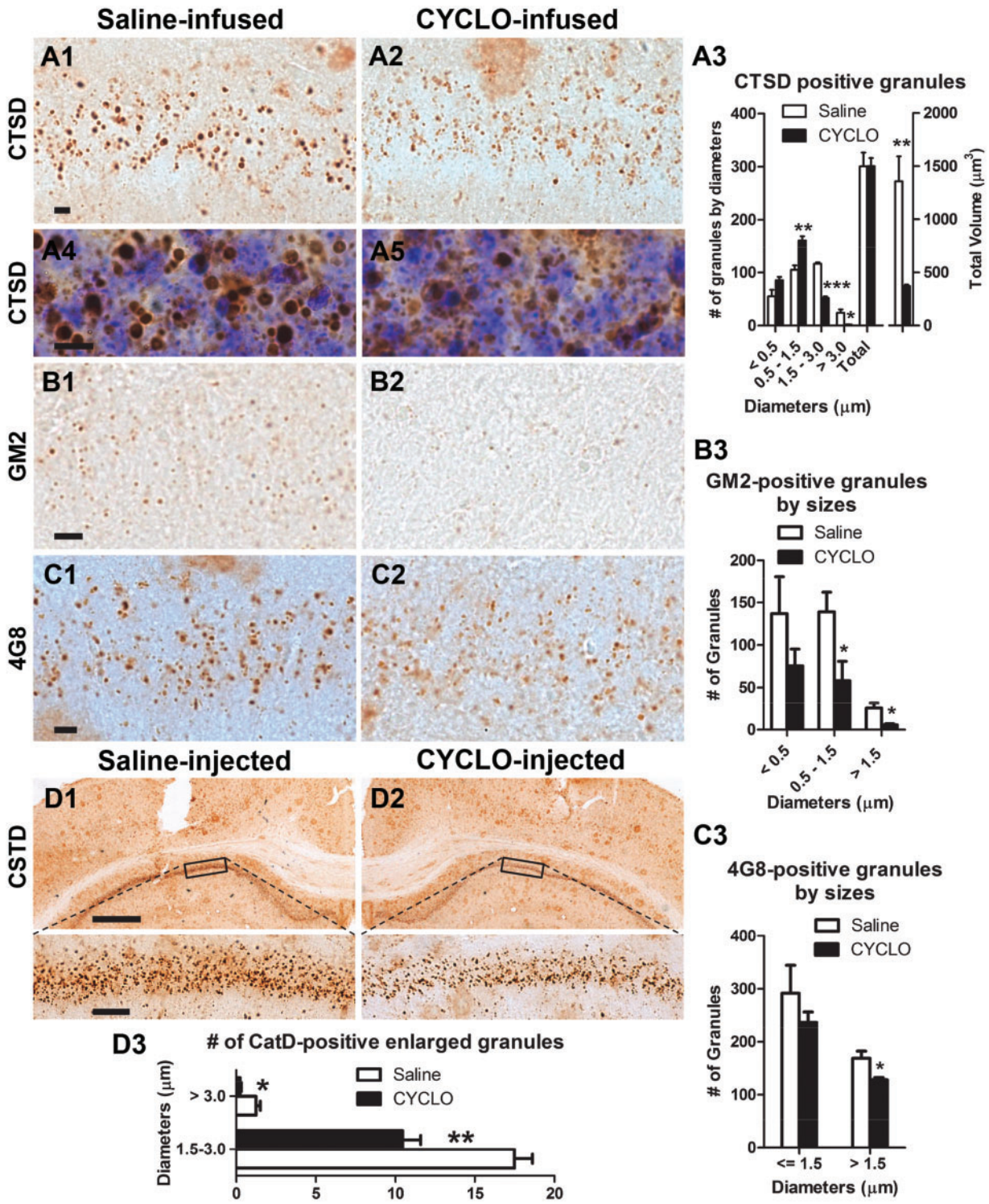

Figure 1. CYCLO intracranial administration reduces the number of giant autolysosomes and associated GM2- or 4G8-signals in the hippocampal CA1 sector in TgCRND8. (**A–C**) TgCRND8 mice (8∼9-mo-old) were treated (ICV infusion) with CYCLO or Saline for two weeks. Brain sections were immunostained with an antibody directed against CTSD (A), ganglioside GM2 (B) or the 4G8 antibody (C). (**A3**, **B3**, **C3**) Intracellular CTSD-, GM2- or 4G8-positive granules (31,39) in the CA1 pyramidal cell layer were quantified. (A3) demonstrates both the number (Left) and the total autolysosomal/lysosomal volume (Right) of CTSD-positive granules. Values are the mean ± SEM for each group ($n = 4$ mice per treatment). Significant differences between the two treatment groups were analyzed by two-tailed Student's *t*-test. $^{*}P < 0.05$, $^{**}P < 0.01$, $^{***}P < 0.001$. (**A4**, **A5**) High magnification images were taken from CTSD immunostained sections which were counterstained with cresyl violet. (**D**) CYCLO (20%, 0.3 μl) (**D2**) or saline (**D1**) was injected into the right or left hippocampus of TgCRND8 mice (8-mo-old), respectively. Seven days later, the mice were sacrificed and coronal brain sections were immunostained with the anti-CTSD antibody. Images were taken from both injection sides. Bottom panels are higher magnification of boxed areas delineated in the images above. High magnification images were used for quantitation of CTSD-positive granules (D3). Values are the mean ± SEM for each injection side which were analyzed by two-tailed Student's *t*-test ($n = 4$ TgCRND8 mice). $^{*}P < 0.05$, $^{**}P < 0.01$. Scale bars: 10 μm (A, B, C); 500 μm (D1, D2, top); 50 μm (D1, D2, bottom).

Table 1. Summary of CYCLO administrations to TgCRND8 and wild type (WT) mice

Experiment	Administration route	No. & sex of TgCRND8 (saline/CYCLO)	No. & sex of WT (saline/CYCLO)	Age (mo)	Background strain	CYCLO dosage
1	IP injection	1F, 2M/1F, 2M	2F, 2M[a]	16–17	129S6	4000 mg/kg, every other day, total 14 days
2	IP injection	2F, 4M/2F, 5M	2F, 3M/3F, 3M	8–9	129S6	4000 mg/kg, every other day, total 14 days
3	ICV infusion	1F, 2M/1F, 3M		14–15	129S6	40 mg/kg/day, total 14 days
4	ICV infusion	2F, 2M/1F, 3M	2F, 4M/2F, 3M	8–9	129S6	40 mg/kg/day, total 14 days
5[b]	ICV infusion	1F, 3M/2F, 3M	2F, 3M/2F, 3M	8–9	129S6	40 mg/kg/day, total 14 days
6	ICV infusion	2F, 4M/2F, 5M	2F, 3M/2F, 3M	8	129S6	40 mg/kg/day, total 14 days
7	Intra-hippocampal injection	0/6M		16–17	129S6	0.06 or 0.12 mg, one-time injection, 2 or 7 days
8	Intra-hippocampal injection	4M		8	129S6	0.06 mg, one-time injection, 7 days
9	ICV infusion		2F, 3M/2F, 3M	6	C57BL/6	40 mg/kg/day, total 14 days
Total		**66**	**56**			

IP = intraperitoneal; ICV = intracerebroventricular; mo = month.

[a]WT mice not receiving injections served as the control.

[b]Mice in this group were primarily assigned for EM study, but hemibrains were also used for biochemical analysis such as ELISA and immunoblotting.

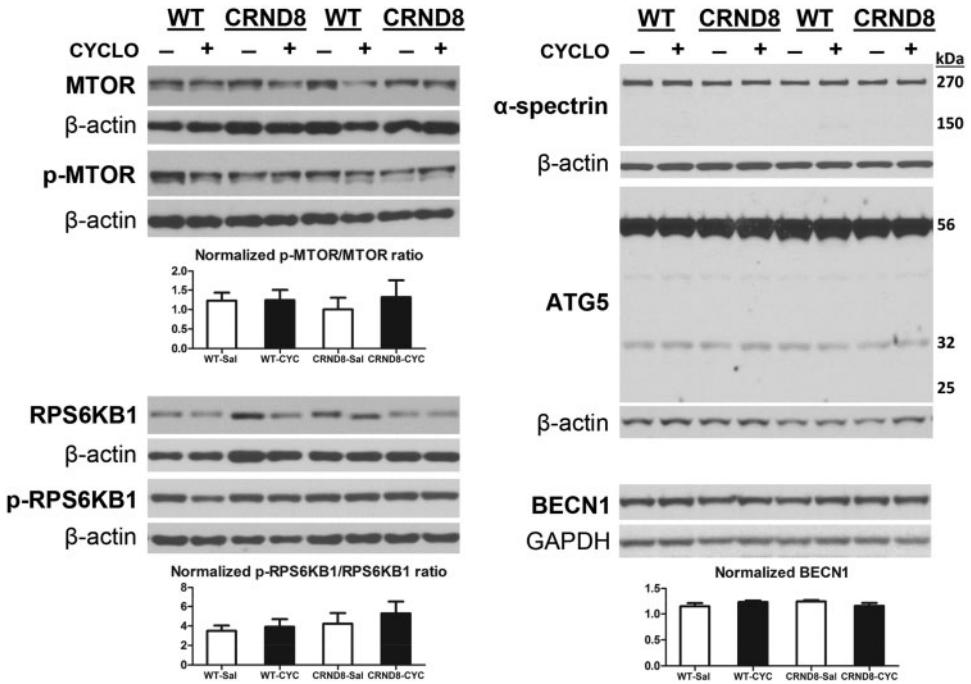

Figure 2. CYCLO ICV infusion does not have effects on brain protein levels of autophagy induction markers. TgCRND8 (CRND8) and WT mice (8∼9-mo-old) were treated (ICV infusion) with CYCLO or Saline for two weeks. Equal amounts of proteins from brain homogenates were subjected to SDS-PAGE and processed for WB with antibodies directed against total MTOR, p-MTOR, total RPS6KB1, p-RPS6KB1, α-spectrin, ATG5 or BECN1, and representative blots are shown. Quantification of blots is shown below the corresponding blot(s). Values are the mean ± SEM for each group ($n = 4$-5 mice per genotype per treatment). Significant differences between the two treatment groups of each genotype were analyzed by two-tailed Student's t-test. The β-actin or GAPDH blots serve as loading controls.

measured the levels of ATG5 and detected no changes in the levels of the 56 kDa ATG5-ATG12 conjugate, the 32 kDa full-length ATG5, and the 24 kDa CAPN-cleaved fragment. These data indicate that CAPN activation after CYCLO treatment is minimal. In addition, we did not detect differences in the levels of JNK1 and phospho-JNK1 (i.e. activated JNK1) between CYCLO- and saline-treated samples (not shown). Phospho-JNK1 is involved in another MTOR-independent autophagy activation pathway where phosphor-JNK1 is capable of stimulating autophagy induction through phosphorylating Bcl-2, leading to disruption of the Bcl-2/BECN1 (Beclin-1) complex, thereby removing the inhibitory effect of Bcl-2 on BECN1 (46,49).

Furthermore, BECN1, an autophagy effector essential for different steps of the autophagic process including autophagosome biosynthesis and maturation (50), also exhibited similar levels in samples from both treatment groups (Fig. 2). Taken together, these observations suggest that CYCLO treatment does not affect autophagy induction *in vivo*.

Short-term ICV administration of CYCLO increases the levels and activity of cathepsins

Given the absence of alterations in the stage of autophagy induction after CYCLO treatment, we next assessed the possible effects of CYCLO on the stage of lysosomal degradation by examining the levels of CTSB/cathepsin B and CTSD, belonging to the families of cysteine and aspartyl proteases respectively. Interestingly, compared to saline-treated samples, CYCLO-treated samples exhibited elevated levels of proform/single chain and 30 kDa mature forms of CTSB (Fig. 3A). Similarly, there was a trend of elevation in the levels of CTSD proform (46 kDa) and mature forms, including 42 kDa (single chain) and 30 kDa (heavy chain of the double-chain form) (51) in CYCLO-treated samples (Fig. 3B). To reveal the functional consequence of these alterations in CTSB and CTSD protein levels, we investigated enzymatic activities of CTSB and CTSD (Fig. 3C). Although CTSB activity was not detectably altered by CYCLO-treatment (Fig. 3C, left), CTSD activity was elevated in CYCLO-treated samples, particularly in the TgCRND8 group (Fig. 3C, middle). Normalization of the CTSD activity with the protein signals on the immunoblot to yield CTSD specific activity also revealed a similar trend (Fig. 3C, right). Together, CYCLO treatment induces a mobilization of lysosomal proteases, which would be expected to enhance lysosomal proteolysis, as previously shown using another treatment approach (39).

To obtain insights into the underlying mechanism(s) for the increases in cathepsin levels and activity, we first examined if CYCLO induced alterations of TFEB and TFE3, members of the MiT family of transcription factors that drive the expression of most lysosomal genes, including cathepsins, as well as a number of other autophagy genes (52,53). By immunoblotting and immunostaining for TFEB (Supplementary Material, Fig. S1) and TFE3 (Supplementary Material, Fig. S2), we were unable to detect differences in their protein levels (including the patterns of posttranslational modifications) and subcellular distributions between samples from saline- vs. CYCLO-infused brains. In particular, there were no detectable changes in the cytoplasmic and nuclear staining pattern of either TFEB (Supplementary Material, Fig. S1B) or TFE3 (Supplementary Material, Fig. S2B) after CYCLO treatment, suggesting that CYCLO did not enhance TFEB or TFE3 nuclear translocation, which is considered to be important for TFEB/TFE3 activation and the downstream induction of autophagy-lysosomal genes including cathepsins (54). Therefore, these data suggest that the TFEB/TFE3 mechanism is unlikely to explain CYCLO-induced cathepsin increases.

It has been reported that CTSB, CTSD and some other lysosomal proteins are binding partners of NPC1, which is downstream of the nuclear receptors LXR/RXR, and that, in fibroblasts from NPC patients, lowered NPC1 levels correlate with mature CTSD decrease while increasing NPC1 levels elevates CTSD activity (55,56). These findings suggest that NPC1 protein plays a role in regulating cathepsin levels and activity. ABCA1, a lipid transporter for the lipidation of apolipoproteins, is another downstream protein of LXR/RXR and also regulated by NPC1 and CTSD (57–60). Quantitative immunoblot analysis for NPC1 and ABCA1 revealed that although saline-infused WT and TgCRND8 mice did not differ, CYCLO-infusion substantially increased the levels of NPC1 and ABCA1 in the brains of both WT and TgCRND8 (Fig. 3D and E). Together, CTSD, CTSB, NPC1 and ABCA1 proteins responded to CYCLO treatment in the same trend and similar elevation magnitudes. To test whether or not the CTSD response to CYCLO is NPC1-dependent as suggested by previous studies (55,56), we knocked down NPC1 in cultured N2a cells and found that CYCLO could still induce changes in the levels of CTSD under the conditions that NPC1 protein was significantly knocked down (Supplementary Material, Fig. S3A), which questions the role of NPC1 but could nevertheless still argue that the remaining low level of NPC1 is sufficient to mediate a CTSD response. Thus, we further tested CYCLO treatment in NPC1-knockout mouse neuronal cells without or with the reintroduction of NPC1 through transfection of a NPC1 construct (Supplementary Material, Fig. S3B). Consistent with the finding from CYCLO-treated brain homogenates (Fig. 3D), CYCLO treatment in NPC1-reintroduced NPC1-KO neuronal cells increased the levels of NPC1 (Supplementary Material, Fig. S3B1, top). Quantitative analysis indicates that there is a significant difference in the level of CTSD 30 kD mature form between the untreated NPC1-KO cells (i.e. “NPC1 DNA-/CYCLO-”) and the NPC1-KO cells transfected with NPC1 and treated with CYCLO (i.e. “NPC1 DNA+/CYCLO+), but no difference between CYCLO-treated and -untreated NPC1-KO cells without NPC1-reintroduction (Supplementary Material, Fig. S3B2). The data together suggest that NPC1 is capable of facilitating CYCLO-induced changes in CTSD even if it may not be solely responsible, and other molecules may also be possibly involved.

Short-term ICV administration of CYCLO delays autophagosome maturation

Unexpectedly, we also observed that levels of LC3-II, SQSTM1/p62 and ubiquitinated proteins rose significantly in both WT and TgCRND8 mice receiving CYCLO (Fig. 4). Elevated LC3-II may suggest either enhanced autophagy induction or impaired lysosomal clearance capacity, or both (61). Our observations that CYCLO did not induce autophagy and also seems to enhance lysosome degradative function raised the alternative possibility that autophagosome-lysosome fusion may be delayed. To investigate this possibility, we first performed immunofluorescence labeling to localize accumulated SQSTM1. In hippocampus (Fig. 5A1) and cortex (not shown) of both CYCLO-infused WT and TgCRND8 mice, SQSTM1 immunoreactive structures appeared as large intracellular clumps, which, at high magnification, were vacuolated inclusions (Fig. 5A1, insets). Quantitative analysis revealed that SQSTM1-clumps were hardly detectable in saline-infused brains but were numerous in CYCLO-infused brains (Fig. 5A2). To verify whether SQSTM1-clumps were associated with organelles of the autophagy pathway, we double-labeled them with a SQSTM1 antibody and an antibody specific for polyubiquitin linked at the K63 residue that selectively labels proteins degraded by macroautophagy (61). As shown in Figure 5B, most, but not all, SQSTM1-clumps colocalized with the K63 signal, suggesting their location within the autophagic pathway. Further double-immunofluorescence labeling with SQSTM1 and CTSD antibodies revealed only minimal colocalization of SQSTM1 and CTSD signals (Fig. 5C). Quantitative colocalization analysis with Pearson’s Correlation Coefficient indicated a high degree of colocalization between SQSTM1 and K63 signals and minimal colocalization between SQSTM1 and CTSD signals (Fig. 5D), indicating that CYCLO-enhanced SQSTM1 immunoreactivity is minimally associated with autolysosomes/lysosomes (Fig. 5C) and mainly with autophagosomes.

To confirm the CYCLO-induced accumulation of autophagosomes, we carried out ultrastructural analyses on brains from WT and TgCRND8 mice after saline or CYCLO ICV administration (Fig. 6). In saline-treated WT mice, small autolysosomes (including small lipofuscin granules—i.e. pigmented autolysosomes)

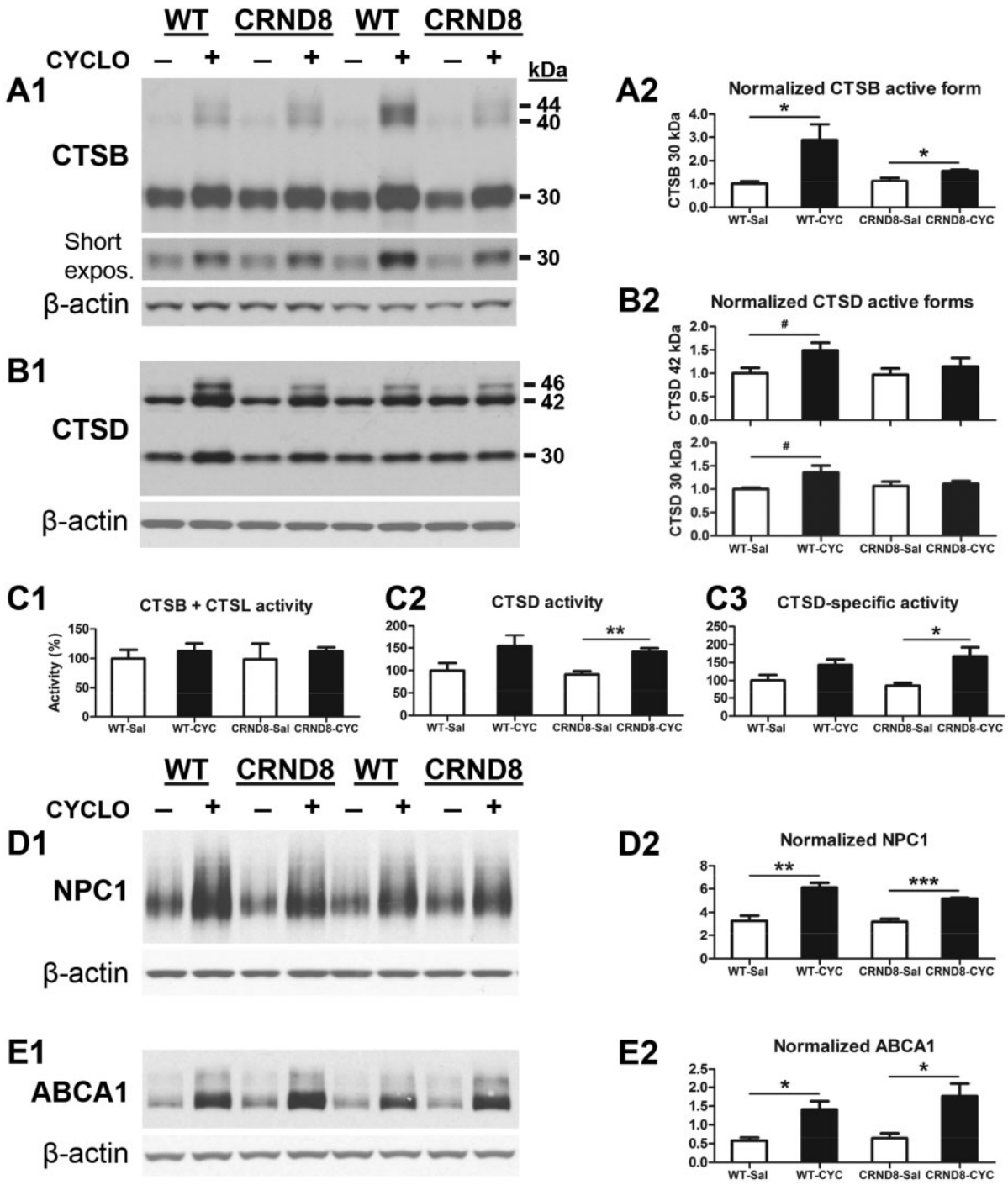

Figure 3. CYCLO ICV infusion enhances brain protein levels and activity of cathepsins and protein levels of NPC1 and ABAC1. TgCRND8 (CRND8) and WT mice (8∼9-mo-old) were treated (ICV infusion) with CYCLO or Saline for two weeks. (**A**, **B**) Equal amounts of proteins from brain homogenates were subjected to SDS-PAGE and processed for WB with antibodies directed against CTSB, CTSD, NPC1 or ABCA1 and representative blots are shown (**A1**, **B1, D1, E1**). Quantification of blots is shown on the right next to the corresponding blot (**A2**, **B2, D1, E1**). (**C**) Results of enzymatic activity assays for CTSB and CTSL (**C1**) or CTSD (**C2**) activities in brain homogenates. (**C3**) The CTSD activity shown in (**C2**) was recalculated against the β-actin normalized CTSD values obtained from the immunoblots probed with anti-CTSD and anti-β-actin (B1) to yield the CTSD-specific activity for which the combined values from the three mature forms (i.e. 42-, 32- and 14-kDa) were used for the calculation. Values for WB densities or enzymatic activities are the mean ± SEM for each group ($n = 4$-5 mice per genotype per treatment). Significant differences between the two treatment groups of each genotype were analyzed by two-tailed Student's *t*-test. $^{*}P < 0.05$, $^{**}P < 0.01$, $^{***}P < 0.001$, $^{\#}P < 0.06$. The β-actin blots serve as loading controls.

and lysosomes were readily detected in neuronal perikarya of the hippocampal pyramidal cell layer but autophagosomes were rarely detected (Fig. 6A). Saline-treated TgCRND8 displayed the characteristic appearance of giant autolysosomes/lipofuscin granules (Fig. 6B) and smaller numbers of normal-sized autolysosomes, consistent with earlier findings (31,39). Autophagosomes and lysosomes were rarely seen in affected TgCRND8 neuronal populations. By contrast, in both CYCLO-infused WT (Fig. 6C) and

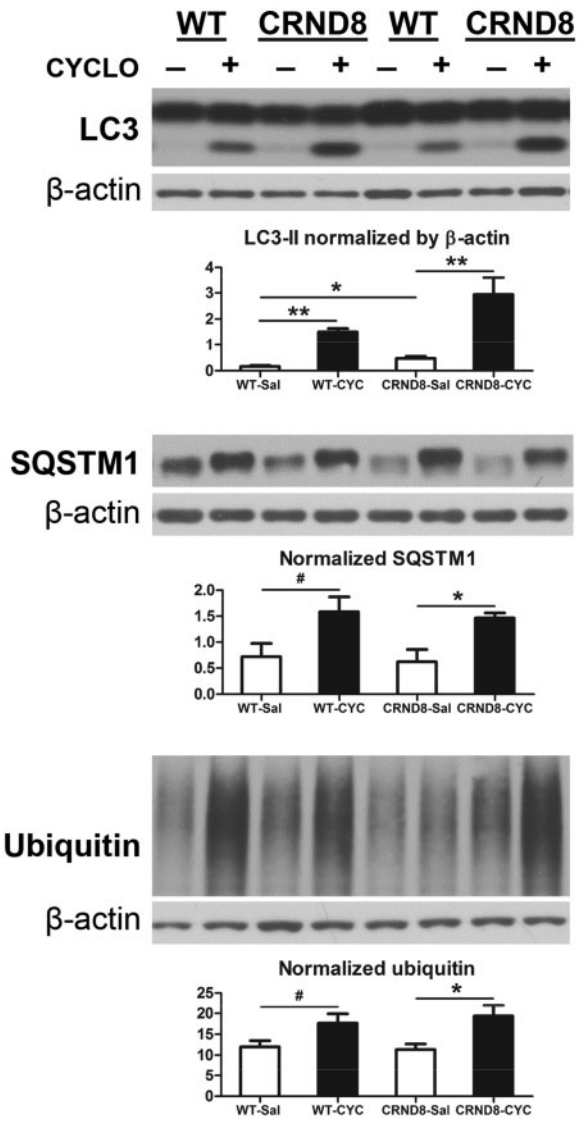

Figure 4. CYCLO ICV infusion elevates brain protein levels of LC3-II, SQSTM1 and ubiquitinated proteins. TgCRND8 (CRND8) and WT mice (8∼9-mo-old) were treated (ICV infusion) with CYCLO or Saline for two weeks. Equal amounts of proteins from brain homogenates were subjected to SDS-PAGE and processed for WB with antibodies directed against LC3, SQSTM1, or ubiquitin, and representative blots are shown. Quantification of blots is shown below the corresponding blot(s). Values are the mean ± SEM for each group ($n = 4$-5 mice per genotype per treatment). Significant differences between the two treatment groups of each genotype were analyzed by two-tailed Student's *t*-test. $^{*}P < 0.05$, $^{**}P < 0.01$, $^{\#}P < 0.06$. The β-actin blots serve as loading controls.

TgCRND8 mice (Fig. 6D), we readily detected autophagosomes, identified by a bordering double membrane and a content of recognizable organelles (e.g. mitochondria) and/or other cytoplasmic constitutes with a light electron density similar to that in the cytoplasm. Autophagosomes were markedly increased in number, as shown by morphometric analysis (Fig. 6E). In addition, we detected a population of atypical irregularly shaped autophagosomes (Fig. 6C and D, # signs) not observed in saline-treated mice, usually with double membranes and a content of multiple small autophagic vacuoles of varying electron density. Their number was usually smaller than those typical autophagosomes. In some cases, these profiles were present in clusters and appeared to be in varying stages of fusion (Fig. 6C2). Immuno-EM with the anti-CTSD antibody revealed gold particles within some of the vacuoles in the larger multivesicular structures (Fig. 6C2, inset). The appearance of these structures likely reflects repeated cycles of autophagic sequestration of smaller groups of autophagosomes and early autolysosomes and in some cases, additional fusion events occurring between these clusters of autophagosomes. These events yield the formation of large multi-vacuolated autophagosomes with minimal levels of cathepsin immunoreactivity. Collectively, these findings indicate that CYCLO ICV infusion impairs maturation of autophagosomes leading to their accumulation and subsequent attempts to clear them by continuous cycles of macroautophagic sequestration, which contrasts with the normally rapid clearance of autophagosomes through fusion with lysosomes (62).

To further verify if CYCLO could induce a delay in autophagosome-lysosome fusion, as suggested by earlier *in vitro* studies (63), we transfected mouse hepatocytes with a mCherry-eGFP-LC3 DNA construct to monitor the formation, maturation and clearance of autophagosomes (61,64) in the absence or presence of CYCLO. This LC3 reporter is capable of distinguishing autophagosomes which fluoresce yellow-green, from autolysosomes, which fluoresce orange-red due to quenching of the acid-sensitive eGFP fluorescence upon luminal acidification after autophagosome-lysosome fusion. As shown in Supplementary Material, Figure S4A, untreated cells exhibited predominantly red-LC3 signal reflecting autolysosomes and suggesting normal autophagosome-lysosome fusion. By contrast, CYCLO-treated cells exhibited a predominant LC3-positive puncta population that fluoresced green to orange-yellow indicating that they are early and late autophagosomes evidencing minimal fusion with lysosomes. Quantitative colocalization analyses confirmed a higher degree of colocalization between the red and green signals (Supplementary Material, Fig. S4B1) and thus increased number of autophagosomes but decreased numbers of autolysosomes (Supplementary Material, Fig. S4B2) in CYCLO-treated cells compared with untreated cells.

CYCLO ICV infusion induces similar autophagic responses in the brain of wild-type C57BL/6 mice

As shown in Table 1, the mice used in Experiments 1–8 were on a 129S6 genetic background. To determine if CYCLO-induced autophagic changes in the mouse brain are specific to the 129S6 strain, we also investigated effects of CYCLO on the C57BL/6 mouse line. Using the same ICV infusion protocol, we found that CYCLO elevated protein levels of NPC1, CTSB and LC3-II (Supplementary Material, Fig. S5A) and SQSTM1 immunoreactivity (Supplementary Material, Fig. S5B) and increased numbers of autophagosomes in the brains of C57BL/6 mice (Supplementary Material, Fig. S5C), all similar to what is seen in mice with the 129S6 genetic background, although the atypical clustered/fused autophagosomes shown in Figure 6C2 were not observed. These data suggest that CYCLO has similar effects on *in vivo* autophagy in both 129S6 and C57BL/6 mouse brains but somewhat less robust accumulation of autophagosomes in the C57BL/6 mouse background.

Short-term CYCLO treatments in TgCRND8 mice do not alter brain amyloid plaque load, Aβ levels and APP processing

CYCLO systemically administered to a mouse AD model between ages 7 and 120 days was shown to prevent amyloid

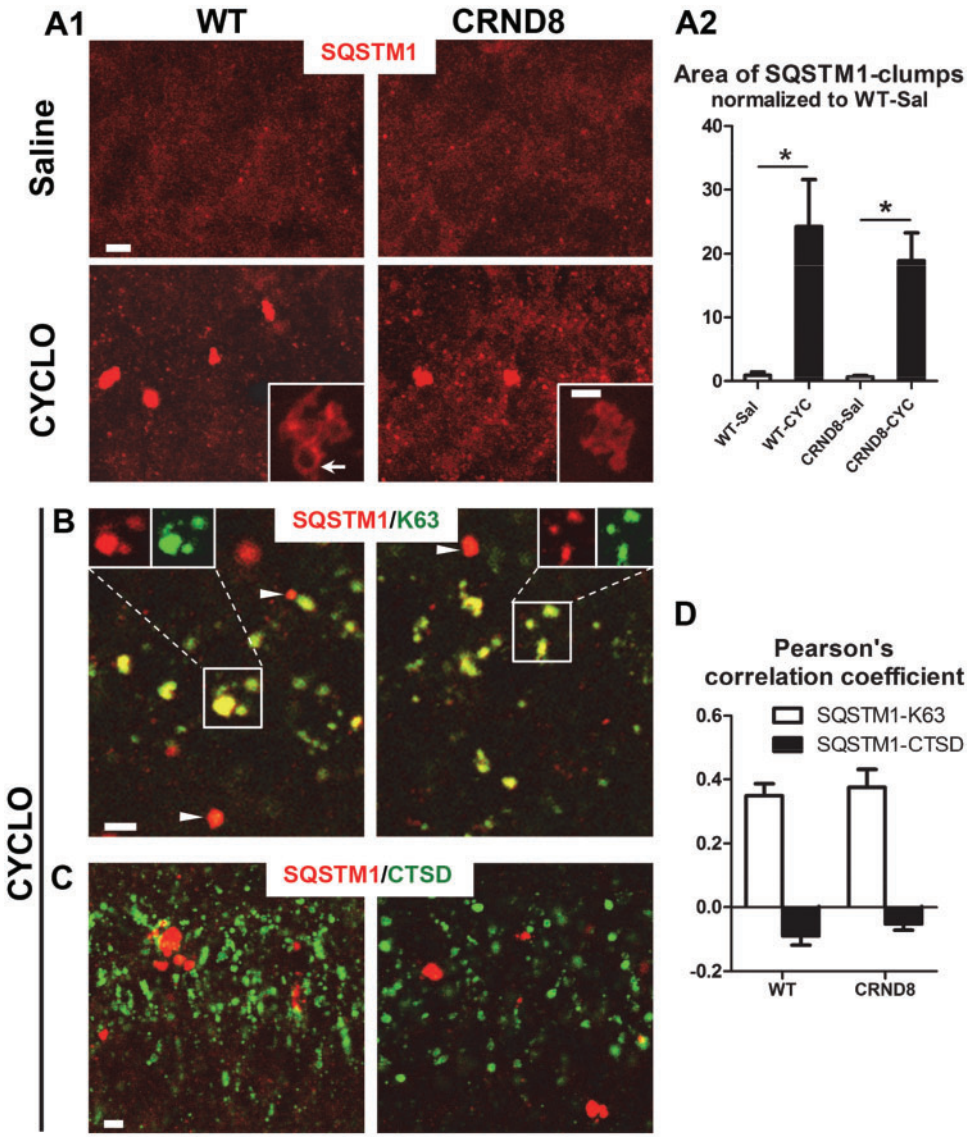

Figure 5. CYCLO ICV infusion induces SQSTM1 accumulation in autophagosomes. TgCRND8 (CRND8) and WT mice (8∼9-mo-old) were treated (ICV infusion) with CYCLO or Saline for two weeks. (**A1**) Brain sections were immunostained with an anti-SQSTM1 antibody and confocal microscopy images from the hippocampal CA1 sector are shown. (A1 Insets) High magnification single optical plane images depict the detail of SQSTM1-positive clumps such as the hollow appearance (arrow). (**A2**) SQSTM1 clumps were quantified and expressed as relative area of immunoreactivity normalized to that of WT-saline condition. Values are the mean ± SEM for each group ($n = 4$ mice per treatment). Significant differences between the two treatment groups of each genotype were analyzed by two-tailed Student's *t*-test. *$P < 0.05$. (**B, C**) Brain sections were double-stained for SQSTM1 and an autophagosome/autolysosome marker, ubiquitin linked at the K63 residue (K63) (B) or an autolysosome/lysosome marker, CTSD (C), and confocal images taken from the hippocampal CA1 pyramidal cell layer are shown. Examples showing SQSTM1-only signal without apparent colocalization with the K63 signal are indicated by arrowheads (B). (**D**) Quantitative colocalization analysis with Pearson's Correlation Coefficient for the SQSTM1/K63 and the SQSTM1/CTSD pairs. Values are the mean ± SEM for each group ($n = 4$ mice per treatment). Scale bar: 5 μm (A, B, C); 2 μm (A, Insets).

plaque formation and reduce Aβ levels (40). Although we did not expect the short-term CYCLO administration to alter amyloid burden in TgCRND8 in light of previous data on slow clearance of plaque amyloid (65), we confirmed that 14-day treatment of CYCLO via either IP injection (Supplementary Material, Fig. S6) or ICV infusion (Supplementary Material, Fig. S7) (Table 1) did not significantly alter the brain amyloid plaque load, Aβ levels (mainly determined by deposited β-amyloid in adult TgCRND8), or APP processing (Supplementary Materials, Figs. S6 and S7). Amyloid plaque load quantified in hippocampal or cortical regions of sections immunostained with antibodies specific for Aβ40 (Supplementary Material, Fig. S6A1) or Aβ42 (Supplementary Material, Fig. S6A2) and with 4G8 antibody (Supplementary Material, Fig. S7A) was not significantly different in CYCLO- and saline-treated TgCRND8 mice (Supplementary Materials, Figs. S6B and S7B). Similarly, ELISA measurements of Aβ40 and Aβ42 (Supplementary Materials, Figs S6C and S7C) and quantitative immunoblot analyses with antibody 6E10 to assess APP holoprotein, Aβ, β-CTF and a 25 kDa band suggestive of Aβ oligomers revealed no effects of CYCLO (Supplementary Materials, Figs S6D and E, S7D and E).

Discussion

We observed that short-term CYCLO treatment in affected TgCRND8 mice reduces the numbers of giant autolysosomes

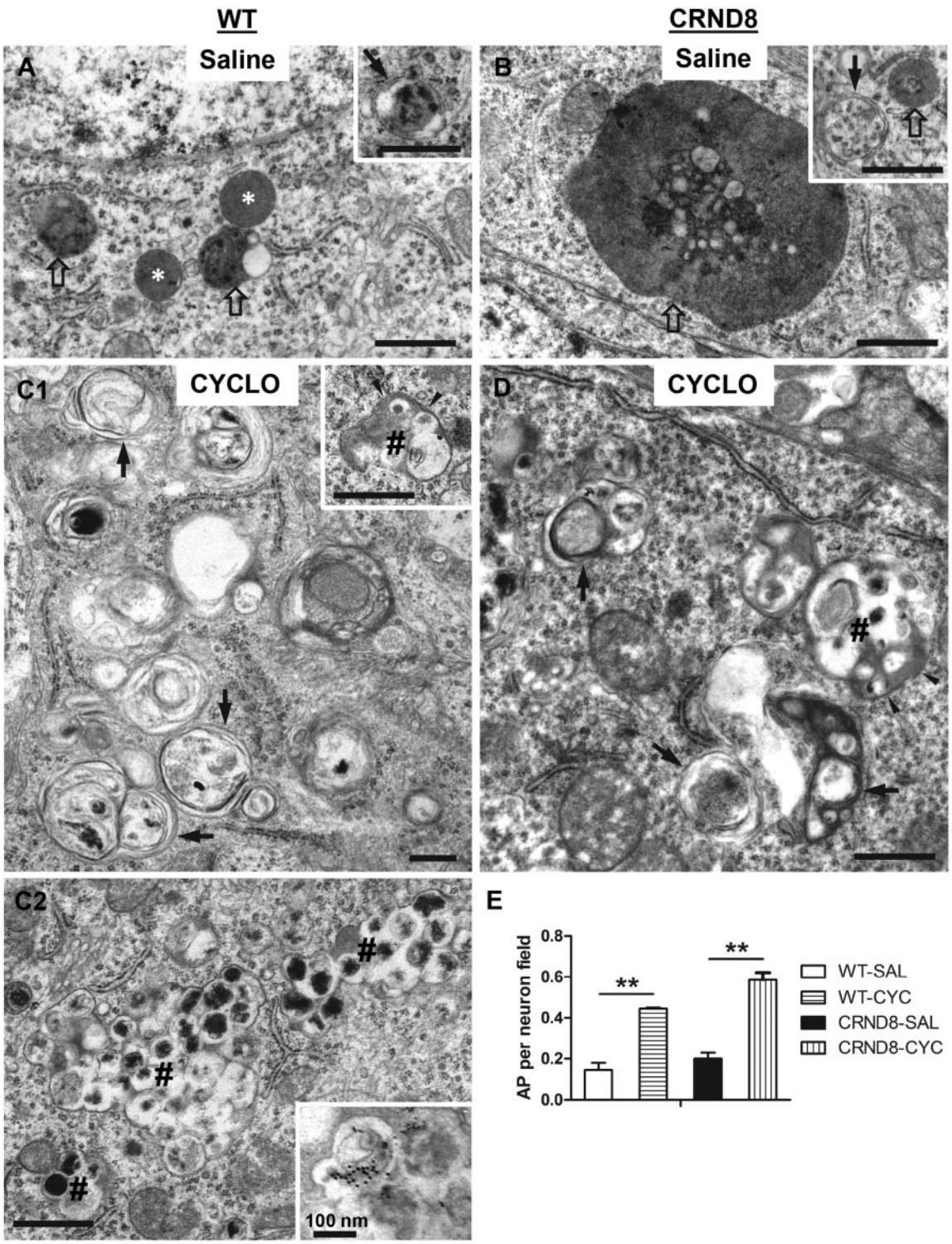

Figure 6. CYCLO ICV infusion increases the number of autophagosomes. TgCRND8 (CRND8) and WT mice (8~9-mo-old) were treated (ICV infusion) with CYCLO or Saline for two weeks. (**A–D**) Brain sections were processed for EM analysis and images taken from the pyramidal cell layer of the CA1 sector are shown. Arrows = autophagosomes, defined as double-membrane-bound vacuoles with low electron density and relatively "intact" contents (e.g. recognizable organelles or membrane). Empty arrows = autolysosomes, characterized by single-limiting membrane with higher electron density and amorphous heterogeneous contents. White stars = lysosomes, defined as small round/oval vacuoles with single-limiting membrane, homogenous content and being devoid of undigested material. # signs = multi-vacuolated autophagosomes, which exhibit recognizable double-membrane in some areas (arrowheads) and consist of multiple small vacuoles. (**C2**) An example for clusters of these multi-vacuolated autophagosomes—3 such profiles can be identified from bottom-left to top-right. Inset: immune-EM with anti-CTSD antibody showing the appearance of gold particles within the multi-vacuolated autophagosomes similar to those marked with # in (C2). (**E**) EM images (19,000X) were taken from the CA1 pyramidal cell layer. The numbers of autophagosomes in the neuronal perikarya were counted for quantitative analysis (n = 2-3 mouse brains per genotype per condition; 1-2 tissue blocks per brain; average 40 images per tissue block). Significant differences were analyzed by one way ANOVA followed by post hoc Bonferroni's multiple comparisons test. $^{**}P < 0.01$. Note: those multi-vacuolated autophagosomes were not included in this quantitative analysis. Scale bars: 500 nm. AP = autophagosome; AL = autolysosome; SAL = Saline; CYC = CYCLO.

and 4G8- or GM2-positive vacuoles identified as autolysosomes in previous studies (31,39). Amelioration of intralysosomal accumulations of Aβ-immunoreactive material and lipids in TgCRND8 is consistent with CYCLO effects on reducing lysosomal storage in several disease models, including NPC (9,13), neuronal ceroid lipofuscinosis (45) and retinal degeneration (66), even though CYCLO does not correct lysosomal storage in certain disease models, such as GM1 gangliosidosis and mucopolysaccharidosis (MPS) type IIIA (9).

To the best of our knowledge, this is the first study to characterize the effects of CYCLO on autophagy function *in vivo* in the brain and to evaluate all major steps in the autophagy pathway. While CYCLO treatment did not alter autophagy induction, it exerted two major actions on autophagy that can explain its salutary effects on lysosomal function. Firstly, CYCLO elevates protein levels of pro- and mature-forms of CTSB and CTSD, suggesting a mobilization effect on the lysosomal enzyme biosynthesis and processing. CYCLO also increases enzymatic activity of CTSD. The consequence of such changes is expected to enhance the lysosomal proteolytic function and therefore the clearance of accumulated substrates such as Aβ. This is supported by a regression analysis of CTSD enzymatic activity and the number of 4G8-positive granules in the CA1 pyramidal cell layer (Supplementary Material, Fig. S8) which shows statistically significant correlation between increased CTSD activity and reduced numbers of 4G8-positive granules. Similarly, previous studies have found that cyclodextrin treatment in cell cultures increases the degradation of long-lived proteins mediated by chaperone mediated autophagy and macroautophagy through its effect on membrane lipid composition that modulates substrate binding on, and uptake into, the lysosomes (67). While we did not detect changes in CTSB activity by CYCLO, a previous *in vitro* study in cell cultures using a fluorescence microscopic imaging approach with Magic Red CTSB to detect CTSB activity *in situ* has found that CYCLO elevates the CTSB activity in NPC1-deficient cells (33).

Consistent with improved cathepsin function, we found that CYCLO elevates protein levels of NPC1 and ABAC1, as also seen earlier by others (3,40). As shown in Figure 7, cholesterol is a source of oxysterols which are elevated by CYCLO (3) when cholesterol is effluxed from endo-lysosomal compartments to sites of oxysterol synthesis in ER and other organelles. Oxysterols are endogenous ligands for the nuclear receptors LXR/RXR (68,69) that enhance the expression of NPC1 (56,70) and ABCA1 (3,71) among other downstream genes. NPC1, a binding partner of CTSB, CTSD and some other lysosomal proteins, is capable of regulating cathepsin levels and activities (55). In addition, CTSD positively regulates ABCA1 expression (58,72). Enhanced ABCA1 in turn facilitates APOE lipidation and, potentially, APOE-mediated Aβ clearance (57,71,73–75). Together, the increases in NPC1, CTSD and ABCA1 suggest that CYCLO induces a LXR/RXR-involved upregulation and reciprocal interactions of these proteins (55,60), resulting in improved lysosomal degradative function.

CYCLO's second major effect on *in vivo* autophagy is to delay autophagosome maturation at the step of autophagosome-lysosome fusion, which may also involve impairments in autophagosome formation since autophagosomes, if defectively formed, may not undergo a normal fusion process. This conclusion is supported by several lines of evidence. Numbers of autophagosomes, identified ultrastructurally, markedly increase in the absence of a change in autophagy induction. SQSTM1-immunoreactivity accumulates primarily in autophagosomes and only minimally in CTSD-positive autolysosomes/lysosomes. Protein levels of autophagy substrates SQSTM1, LC3-II and ubiquitinated proteins (61,76,77) increase despite improved lysosome function and substrate clearance from lysosomes. Collectively, these observations point to impaired autophagosome maturation occurring prior to the lysosomal degradative step, which we confirmed *in vitro* by showing that CYCLO delayed LC3 flux at the level of autophagosome-lysosome fusion. This effect is in line with *in vitro* observations implicating shifts in levels of cholesterol and other lipids within cellular membranes as a crucial factor in membrane fusion (63) and effects of methyl-β-cyclodextrin in correcting cholesterol content of endolysosomal membranes and normalizing autophagosome maturation (78). We speculate that, in our study, the CYCLO concentration achieved in the interstitial fluid of the brain parenchyma falls into a range (e.g. 0.1–1 mM) that not only mobilizes cholesterol (and other lipids) from endo-lysosomal compartments, but also extracts cholesterol (and other lipids) from cellular membranes (79), resulting in membrane lipid composition changes that alter the distribution or levels of SNARE proteins and oxysterol binding protein related proteins (ORP) mediating autophagosomal-lysosomal fusion (43,80–82). However, it should be noted that such an interpretation for defective fusion does not necessarily exclude possible impairments in autophagosome formation. Indeed, impeded fusion can also be a result of defective autophagosome formation, which could occur because CYCLO-induced membrane lipid composition changes can possibly affect autophagosome membrane building/formation, generating defectively formed autophagosomes. This possibility is supported by the EM observation that there are atypical autophagosomes in CYCLO-treated samples. Similarly, the observation of CYCLO-induced delay in autophagosome-lysosome fusion in mCherry-eGFP-LC3 transfected cells does not necessarily exclude a possible contribution of impaired autophagosome formation as an upstream event. Given that autolysosomes in neurons of TgCRND8 mice are burdened with stored substrates, slowing substrate delivery to lysosomes should reduce competition for lysosomal hydrolases and provide greater access of the pre-existing substrates in lysosomes to these enzymes. A similar mechanism was proposed to explain the improved lysosomal functioning in NPC-deficient cells after autophagosome formation was inhibited pharmacologically (33).

Based on CYCLO's cholesterol mobilizing properties and effects in NPC-deficient models, CYCLO may also directly reduce lysosomal content of cholesterol and other lipids, which are elevated in TgCRND8 mice (31). Lipid and lipoprotein storage impairs lysosomal degradative functions in models of β-amyloidosis and lysosomal storage disorders while partial elimination of stored sphingolipids, such as gangliosides, improves clearance of proteins, including APP metabolites (31,33,39,83–85).

β-cyclodextrin was reported to interact directly with Aβ and inhibit its neurotoxicity in cell cultures (86) although whether or not this interaction occurs *in vivo* in β-amyloid mouse models remains to be investigated. Gangliosides isolated from rat brain lipid rafts are reported to facilitate Aβ oligomerization *in vitro* (87), implying that reducing gangliosides *in vivo* may prevent Aβ oligomerization. In the present study, we observed that CYCLO reduces lysosomal GM2 and Aβ-immunoreactivity, which could include oligomerized Aβ and thus, our observations are compatible with the findings by Kim *et al.* 2006 (87). In any event, the CYCLO-mediated reduction in Aβ-immunoreactivity in lysosomes likely reflects multiple factors including increased cathepsin levels and activities, reduced accumulation of lipids including gangliosides (31,33,39,83–85) as well as possibly

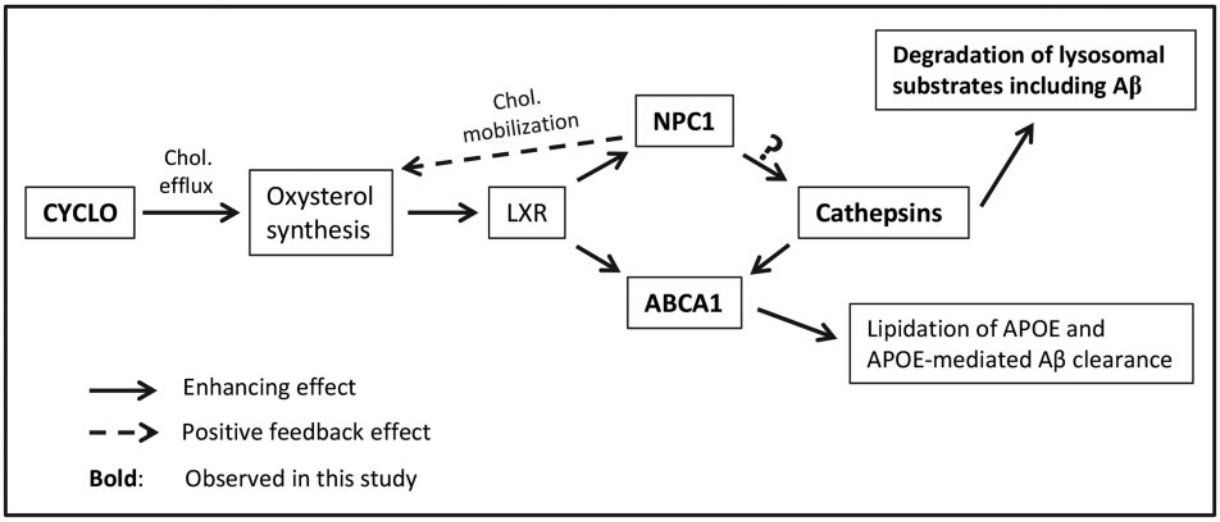

Figure 7. Hypothetical pathways linking CYCLO treatment to the increases of cathepsin levels and activities. CYCLO induces endolysosomal cholesterol efflux to the sites of oxysterol synthesis including ER and mitochondria (100), facilitating the generation of oxysterols (3), endogenous ligands for the nuclear receptors LXR/RXR (68,69), and leading to activation of LXR/RXR. Activated LXR/RXR in turn enhances expression of downstream genes/proteins, including NPC1 and ABCA1 (3,40,56,70,71). Increased NPC1, a binding partner of cathepsins and a regulator of cathepsin expression (55), enhances cathepsin levels and activities (the question mark indicates that NPC1 may not be the only factor in inducing cathepsin changes), leading to improvement in lysosomal degradation of substrates including Aβ and amelioration of lysosomal pathology in TgCRND8. ABCA1 expression is also positively regulated by CTSD (58,72). Increased ABCA1 in turn facilitates APOE lipidation which is important in APOE-mediated Aβ clearance (57,71,73–75). In addition, increases in NPC1, as a lysosomal lipid transporter, also mobilize cholesterol for oxysterol synthesis, constituting a positive feedback loop (101).

diminished formation of more proteolysis-resistant Aβ species, such as oligomers.

The observed effects of CYCLO (Supplementary Material, Fig. S9) in enhancing lysosomal proteolysis and slowing delivery of autophagic substrate into autolysosomes are both expected to contribute to the rescue of lysosomal pathology in TgCRND8 AD model mice. Further studies are necessary to assess whether or not prevention or early intervention delivery paradigms with CYCLO or related derivatives would be a practical avenue for AD therapy, especially given its suspected poor brain uptake and effects on autophagosome maturation, which over long periods could be detrimental to cellular homeostasis due to the gradual build-up of autophagy substrates.

It should be noted that CYCLO has significant effects also on WT mouse brains. Even if CYCLO, a therapeutic agent used clinically, may only be administered in patients with justified needs, the effects of CYCLO on macroautophagy of WT brains observed in the current animal study still raise caution for its detrimental potential, particularly the effects on the autophagosome-lysosome fusion step and possibly the autophagosome formation step as well. Based on the similar alterations in several aspects to those in TgCRND8—elevation of SQSTM1, LC3-II and ubiquitinated proteins, SQSTM1-immunoreactivity accumulation in autophagosomes and accumulation of autophagosomes including atypical ones, we consider that CYCLO may affect macroautophagy in WT brains in a way similar to that in TgCRND8, although other possible mechanism(s) cannot be excluded.

Together, even though clinical trials with intrathecal CYCLO are ongoing in NPC (18) and may be a consideration for atherosclerosis (3) or other conditions, the findings from the current study in mice suggest that animal and human studies with CYCLO should consider careful dosage optimization in order to fine-tune cellular lipid contents to avoid excessive impact on autophagosome maturation, which may affect efficacy and safety. An ideal *in vivo* condition for therapeutic application would be a minimal effect on membrane fusion/autophagosome maturation while still enhancing cathepsin activity to clear stored substrates in the lysosomes. A recent *in vitro* study has found that the inhibitory effect of a given cyclodextrin derivative on autophagosome maturation is correlated positively with its cholesterol binding affinity and the consequent capacity of cholesterol extraction from cellular membranes (44), suggesting that, for a certain cyclodextrin (e.g. the CYCLO), lower doses would decrease its cholesterol binding/extraction capacity and minimize its effect on autophagosome maturation.

Materials and Methods

Animals

All animal procedures were performed following the National Institutes of Health Guidelines for the Humane Treatment of Animals, with approval from the Institutional Animal Care and Use Committee at the Nathan Kline Institute for Psychiatric Research. Animals of both sexes were used in this study. TgCRND8 mice, expressing mutant human APP, Swedish (K670N/M671L) plus Indiana (V717F) mutations, were created on a 129S6/SvEvTac (129S6) strain background by Dr. David Westaway (38). All mice were genotyped by PCR. A total of 66 TgCRND8 and 56 wild type (WT) mice of the same strain at two age groups were used: an “adult” group at 8–9 months and an “old” group at 14–17 months (Table 1). In addition, 10 C57BL/6 WT mice were used (Table 1). All efforts were made to minimize animal suffering and number of animals used.

CYCLO administration to mice

The 2-hydroxypropyl-β-cyclodextrin (CYCLO) used in this study was purchased from Cyclodextrin Technologies Development Inc. (High Springs, Florida, USA), named Trappsol® hydroxypropyl-β-cyclodextrin Endotoxin Controlled or Cyclo powder. It

has been approved by USA Food and Drug Administration (FDA) as a compassionate use Investigational New Drug for two NPC patients receiving intravenous or intrathecal injections (IND104, 114 and IND104, 116). In our studies, CYCLO was dissolved in saline at different concentrations for the three administration routes and mice receiving injections or infusions of saline served as the vehicle control group.

Intraperitoneal (IP) injection (Table 1): In the literature, two doses of CYCLO, 4000 or 8000 mg/kg body weight (BW), have been evaluated for systemic administration of CYCLO in NPC-deficient mouse models (for reviews, see 7, 18) with the 4000 mg/kg dose being most commonly used. We therefore adopted this dose for our IP injection experiment. CYCLO was prepared at 20% (w/v) concentration, injected into the mice every other day, and the mice were sacrificed 15 days after first injection.

Intracerebroventricular (ICV) infusion (Table 1): It has been found that after a single ICV injection of 2 μl of 40% (w/v) CYCLO at 40 mg/kg BW (equivalent to 1.2 mg/30 gram BW) into 49-day-old mice, CYCLO was cleared from the whole CNS with a half-life of ∼6.5 h (8), inferring that the majority of ICV injected CYCLO could be cleared within 24 h. We modified this information for our ICV infusion experiments (Alzet minipump 2002, 0.5 μl/h, total 12 μl/day) to deliver CYCLO at a dose of 40 mg/kg/day (equivalent to 1.2 mg/30 gram BW/day, 0.05 mg/0.5 μl/h) for 14 days into the right lateral ventricle. The implantation of the minipumps was performed following a procedure described previously (88) with the following coordinates for the cannula placement in the lateral ventricle: AP – 0.22 mm to bregma, ML 1.0 mm to bregma, and DV 2.5 mm to cranium. Infused mice were sacrificed 15 days after initiation of infusion.

Intra-hippocampal injection (Table 1): A tiny amount (0.3 μl) of either 20% or 40% CYCLO solution (i.e. 0.06 mg or 0.12 mg, respectively) was injected into the right hippocampus of TgCRND8 brain following a protocol described previously (89). Mice were sacrificed after 2 or 7 days.

Tissue preparation

To obtain tissues for experiments, the animals were anesthetized with a mixture of ketamine (100 mg/kg BW) and xylazine (10 mg/kg BW). Mice for light microscopic analyses were usually fixed by cardiac perfusion using 4% paraformaldehyde (PFA) in 0.1 M sodium cacodylate buffer [pH 7.4, Electron Microscopy Sciences (EMS), Hatfield, PA]. Following perfusion fixation, the brains were immersion-fixed in the same fixative overnight at 4 °C. For transmission electron microscopic (EM) study, 4% PFA was supplemented with 2% glutaraldehyde (EMS). For biochemical analyses, including western blotting (WB) and ELISA, the brains were flash frozen on dry ice and stored at –70 °C. When both morphological and biochemical analyses were to be performed on the same brain, the brain was removed after brief perfusion with saline. One hemisphere was frozen at –70 °C and the other half was immersion-fixed in 4% PFA for 3 days at 4 °C.

Antibodies for immunohistochemistry, WB and ELISA

The following primary antibodies were used in this study: in-house made CTSD pAb (RU4; diluted 1:5000–10 000 for immunohistochemistry (IHC); 1:5000 for WB); in-house made GM2 ganglioside mAb (mouse IgM, cell culture supernatant, produced from the 10–11 hybridoma line provided by Progenics Pharmaceuticals, Inc., Tarrytown, NY; diluted 1:200 for IHC) (90,91), MTOR rabbit mAb (Cell Signaling, #2983s, diluted 1:1000 for WB); p-MTOR pAb (Cell Signaling, #2974s, diluted 1:1000 for WB); RPS6KB1 pAb (Cell Signaling, #9202s, diluted 1:1000 for WB); p-RPS6KB1 pAb (Cell Signaling, #9234s, diluted 1:1000 for WB); α-spectrin mAb (Millipore, #MAB1622, diluted 1:1000 for WB); ATG5 rabbit mAb (Millipore, # MABC137, diluted 1:1500 for WB); JNK pAb (Cell Signaling, # 9252s, diluted 1:1000 for WB); p-JNK mAb (Cell Signaling, # 9255s, diluted 1:1000 for WB); BECN1 pAb (BD Bioscience, #612113, diluted 1:1000 for WB); LC3 pAb (Novus Biological, #NB100-2220, diluted 1:250 for IHC, 1:1000 for WB); SQSTM1 guinea pig pAb (Progen Biotechnik, #GP62-c, diluted 1:200 for IHC, 1:1000 for WB); Lys63-specific ubiquitin rabbit mAb (Millipore, #05-1308, diluted 1:500 for IHC); ubiquitin pAb (Dako, Z0458, diluted 1:2000 for WB); CTSB goat pAb (Neuromics, #GT15047, diluted 1:5000 for WB); NPC1 rabbit mAb (Abcam, #ab134113, diluted 1:1000 for WB); ABCA1 mAb (Abcam, ab18180, diluted 1:500 for WB); TFE3 pAb (Sigma, #HPA023881, diluted 1:200 for IHC, 1:1000 for WB); TFEB pAb (Bethyl Lab, #A303-672A, diluted 1:250 for IHC), TFEB (Bethyl Lab, #A303-673A, diluted 1:1000 for WB). Antibodies directed against APP, Aβ and/or other APP proteolytic species included: 6E10 (mouse mAb specific to human Aβ1-16, diluted 1:1000 for WB) and 4G8 (mouse mAb specific to Aβ17-24, diluted 1:250 For IHC), both from Covance (Emeryville, CA, Catalog No: SIG-39320 and SIG-39220, respectively); and additional mouse mAb—a generous gift of Dr. Marc Mercken (Janssen Pharmaceuticals Corp., Belgium) (92). JRF/cAβ40/10 (specific to Aβ40, diluted 1:500 for IHC, 2.5 μg/ml for ELISA), JRF/cAβ42/26 (specific to Aβ42, diluted 1: 1:500 for IHC, 2.5 μg/ml for ELISA) and HRP conjugated JRF/Aβtot/17 (specific to Aβ1-16, diluted 1:2000 for ELISA). The following secondary antibodies and reagents for immunoperoxidase labeling were purchased from Vector Laboratories (Burlingame, CA): biotinylated goat anti-mouse IgM (BA-2020), M.O.M.™ Immunodetection Kit (BMK-2202), Vectastain ABC kit (PK-4000), and DAB Peroxidase Substrate Kit (SK-4100). The following secondary antibodies for immunofluorescence were purchased from Molecular Probes/Life Technologies (Carlsbad, CA): Alexa Fluor 568-conjugated goat anti-mouse IgG (A11031), Alexa Fluor 488-conjugated goat anti-rabbit IgG (A11034), and Alexa Fluor 568-conjugated goat anti-rabbit IgG (A11036).

Immunolabeling of brain sections

IHC was performed according to the protocols previously described (93). For quantitative analysis of immunostained structures, four sagittal brain sections from each mouse, evenly spaced (400 μm) from the region between Lateral 0.48 mm and 2.16 mm (94) containing the cortex and the hippocampus, were chosen for immunostaining. For quantitative analysis of CTSD, GM2, SQSTM1 or 4G8 stained sections, three 40X digital images were taken from the CA1 area of each section and CTSD-, GM2-, SQSTM1 or 4G8-positive puncta were quantified with AutoMeasure software (Zeiss), and the data were presented in groups based on the diameters of the particles if applicable. CTSD images were also used for calculating the total autolysosomal/lysosomal volume assuming that the granules were spherical. For quantitative analysis of amyloid burden, immunostained sections were scanned and tiled with Mosaix software, and amyloid plaques in the cortex and the hippocampus were quantified with AutoMeasure software (Zeiss, Axiovert 200M microscope). Data are presented as the percent area occupied by the immunoreactivity revealed by the Aβ40, Aβ42 antibody or 4G8. For quantitative colocalization analysis of

double-immunolabeled sections with paired markers (i.e. SQSTM1-ubiquitin K63, SQSTM1-CTSD), 3–4 images of 3–4 sections were taken at 40x from the hippocampal CA1 area using Zeiss LSM880 confocal microscope. Information reflecting colocalization between 2 markers was obtained using the Colocalization Module on the Zen2 Black software (version 2.1) equipped with Zeiss LSM880. Pearson's Correlation Coefficient (default range: -1 to +1) was used to show if there was any colocalization between the paired markers where positive coefficients indicating colocalization while negative coefficients indicating no colocalization.

Western blotting

Samples for WB were prepared by homogenizing brains in a tissue-homogenizing buffer (250 mM sucrose, 20 mM Tris pH 7.4, 1 mM EDTA, 1 mM EGTA) containing protease and phosphatase inhibitors as previously described. (95) Following electrophoresis, proteins were transferred onto 0.2 μm-pore nitrocellulose membranes (Whatman, Florham Park, NJ) at 100 mA for 8–12 h depending on the target protein. The blots were blocked for 1 h in 5% non-fat milk in TBS, rinsed in TBST (TBS + 0.1% Tween-20), then incubated with a primary antibody in 1% BSA/TBST overnight at 4 °C. The membrane was washed and incubated in a HRP conjugated goat-anti rabbit or mouse secondary antibody (Jackson ImmunoResearch Laboratories, West Grove, PA), diluted 1:5000 in 5% milk for 1 h at room temperature. The membrane was again washed and then incubated in a Novex ECL (Invitrogen) for 1 min and exposed to film. Densitometry was performed with Image J and the results were normalized by the immunoblot(s) of given loading control protein(s) (e.g. actin, tubulin).

Ultrastructural analyses

For EM, vibratome sections of the brain were post-fixed in 1% osmium tetroxide. Following alcohol dehydration, sections were embedded in Epon (EMS, Hatfield, PA). One-micron-thick sections were stained with toluidine blue for light microscopic examination and ultrathin sections prepared and stained with uranyl acetate and lead citrate. The material was viewed with a Philips CM 10 electron microscope equipped with a digital camera (Hamamatsu, model C4742-95) aided by AMT Image Capture Engine software (version 5.42.443a). For quantification of autophagosomes and autolysosomes, EM images (19,000X) were taken from the neuronal cytoplasm of the hippocampal CA1 pyramidal cell layer containing autophagic-lysosomal compartments. The images may contain a small portion of the neuronal nucleus but not glial cells. The numbers of autophagosomes and autolysosomes within the neuronal perikaryon were counted, and expressed as the number per image.

Post-embedding IEM with gold-conjugated secondary antibody was performed to detect CTSD signal in neuronal cell bodies using a previously described protocol (88). Ultrathin sections were placed on nickel grids, air-dried, and etched briefly with 1% sodium metaperiodate in PBS followed by washing in filtered double-distilled water and incubated with 1% BSA for 2 h. Sections then were incubated overnight in the anti-CTSD antibody (RU2, 1:1000) in a humidified chamber overnight at 4 °C, washed in PBS, and incubated in a secondary antibody conjugated with 10-nm gold particles (Amersham, Buckinghamshire, UK) for 2 h at room temperature. Grids were washed and briefly stained with uranyl acetate and lead citrate before examination.

Sandwich ELISA

Cerebral Aβ levels were assayed from formic-acid-extracted, hemi-brain sucrose homogenates using an ELISA method in which Aβ was trapped with a mAβ to either Aβ40 (JRF/cAβ40/10) or Aβ42 (JRF/cAβ42/26) and then detected with horseradish peroxidase (HRP)-conjugated JRF/Aβtot/17. The dilution of JRF/Aβtot/17 and samples was optimized to detect Aβ in the range of 50 to 800 fmol ml^{-1}. ELISA signals were reported as the mean +/- SEM of four replica wells in nmol Aβ per gram brain protein (determined with the BioRad DC protein assay), based on standard curves using synthetic Aβ1–40 and Aβ1–42 peptide standards (American Peptide Co. Sunnyvale, CA) (95–97).

Enzymatic activity assays for cathepsins

CTSB and CTSL/cathepsin L activities were assayed as described previously (98). Samples were preincubated in 0.1 M sodium acetate (pH 5.5) containing 1 mM EDTA and 2 mM cysteine-HCl for 5 min for activation. Following the addition of 5 μM Z-Phe-Arg-AMC in 0.1% Brij-35, reaction mixtures were further incubated for 10–30 min at 37° C. Reactions were stopped by addition of 200 μl 0.1 M sodium monochloroacetate in 0.1 M sodium acetate (pH 4.3) and then samples were read in a Wallac Victor-2 spectrofluorimetric plate reader (PerkinElmer Life and Analytical Science Inc., Wellesley, MA). Specificity of hydrolysis by these cathepsins was monitored by inhibition with 1 mM leupeptin and enzymatic activity was expressed as leupeptin-inhibitable hydrolytic activity obtained by subtracting the fluorescent AMC units released in the presence of leupeptin from the total fluorescent AMC units in the acid soluble fraction.

CTSD activity was assayed at 37 °C at pH 4.0 by measuring the release of amc containing peptide, 7-methoxycoumarin-4-acetyl-Gly-Lys-Pro-Ile-Leu-Phe from 7-methoxycoumarin-4-acetyl-Gly- Lys-Pro-Ile-Leu-Phe-Phe-Arg-Leu-Lys(Dnp)-D-Arg-NH2 (BioMol-Enzo, Plymouth Reading, PA), according to the method of Yasuda *et al.* (99). Assays were performed in white microplates in a total volume of 100 μl with and without 3 μg of pepstatin for 1 h. Fluorescence released was read in a Wallac Victor-2 Spectroflurimetric plate reader with a filter optimized for detection of amc standard solution with excitation at 365 nm and emission at 440 nm. However, instead of using amc standard, a quenched standard 7-methoxycoumarin-4-acetyl-Pro-Leu-OH was used for expressing enzyme activity to account for the release of peptide containing amc instead of free amc. Enzyme activity was expressed as the relative amount of quenched standard released per hour per mg protein.

Cell cultures

Reverse transfection with a mCherry-eGFP-LC3 DNA construct in hepatocytes

Mouse hepatocytes (ATCC, Cat#CRL-2390) were maintained in DMEM supplemented with 10% FBS. After trypsinization, cells were plated into 12-well dishes containing a glass cover slip in each well, and transfected with a mCherry-eGFP-LC3 DNA construct (a gift from Dr. Claudio Hetz, Institute of Biomedical Sciences, Faculty of Medicine, University of Chile) (64). After 48 h, the medium was replaced with fresh medium in the absence or presence of CYCLO (1 mM) for 24 h. The cells were then

fixed in 4% PFA and briefly incubated with DRAQ5 (Cell Signaling, #4084) for staining nuclei before examination with a Zeiss LSM880 confocal microscope. High magnification images of positively transfected cells were randomly collected from untreated or CYCLO-treated coverslips, and analyzed for colocalization with the Colocalization Module on the Zen2 Black software (version 2.1). Pearson's Correlation Coefficient (default range: -1 to +1) was used to show if there was any colocalization between the mCherry and the eGFP signals where positive coefficients indicating colocalization while negative coefficients indicating no colocalization. Additionally, colocalization was also analyzed with the Redirection function in NIH Image. The images were inverted and then single cells were selected. After clearing the surrounding area the channels were then split out. The threshold in each channel was then adjusted. The red channel image was highlighted and analyzed using the Set Measurement function with a redirect to the green channel. The Analyze Particle function was used to get the number of vesicles as well as the % of colocalization with the green channel. The data were then collected into Microsoft Excel and a Student t-test was performed to quantify the significance of the differences with or without CYCLO treatment. Anything that had less than 10% colocalization was considered to be not colocalized.

N2a cells

Cells were grown in DMEM supplemented with 10% FBS. The NPC1 was then knocked down in these cells using a combination of all three siNPC1 sequences in the TriFECTa DsiRNA kit (IDT, Cat#mm.Ri.Npc1.13) at 10 nM per sequence dsRNA or 30 nM of control dsRNA. The transfection was done in Optimem with siPort amine for 4 h. The cells were then returned to their growth media for 72 h. After the 72-h period 1 mM CYCLO or PBS was added to the cells for an additional 24 h. The cells were then lysed for immunoblotting.

NPC1 knockout (KO) mouse neuronal cells

The cell line was generated in the lab of Dr. Dobrenis. Cells were grown in Neurobasal medium (Fischer Sci, Cat#12-348-017) supplemented with 3% FBS and B27 (Fisher Sci, Cat#17-504-044) on poly-d-lysine coated cell culture dishes. Cells were transfected serum free for 4 h in Optimem (Fisher Sci, Cat#31985-070) with siPort amine (Fishersci, Cat#AM4502) with either no DNA or 2μg DNA of NPC1 his6 EGFP construct (Addgene, Cat#53521) then put back into growth media. 24 h after transfection the cells were treated with 1 mM CYCLO or PBS vehicle control for an additional 24 h. The cells were then lysed for immunoblotting.

Supplementary Material

Supplementary Material is available at *HMG* online.

Acknowledgements

We are grateful to Nicole Gogel for assistance in article preparation. We are also grateful to Dr. David Westaway (University of Alberta, Canada) for providing a breeding colony of TgCRND8 mice, to Dr. Henry Sershen (Nathan Kline Institute) for providing technical advice on ICV infusion, to the Transgenic Mice Core in the Center for Dementia at the Nathan Kline Institute, headed by Dr. Efrat Levy, for providing some mice for this study and to Drs. Matteo Bordi and Ju-Hyun Lee for thoughtful discussions regarding this project.

Conflict of Interest statement. None declared.

Funding

Alzheimer's Association (IIRG-08-90771 to D.-S.Y.); National Institute of Aging (P01 AG017617 to R.A.N.); Takeda Pharmaceutical Company Limited (to R.A.N.); and National Institute of Child Health and Human Development (R01 HD045561 to S.U.W.).

References

1. Davis, M.E. and Brewster, M.E. (2004) Cyclodextrin-based pharmaceutics: past, present and future. *Nat. Rev. Drug Discov.*, **3**, 1023–1035.
2. Stella, V.J. and He, Q. (2008) Cyclodextrins. *Toxicol. Pathol.*, **36**, 30–42.
3. Zimmer, S., Grebe, A., Bakke, S.S., Bode, N., Halvorsen, B., Ulas, T., Skjelland, M., De Nardo, D., Labzin, L.I., Kerksiek, A., *et al.* (2016) Cyclodextrin promotes atherosclerosis regression via macrophage reprogramming. *Sci. Transl. Med.*, **8**, 333ra50.
4. Lloyd-Evans, E. and Platt, F.M. (2010) Lipids on trial: the search for the offending metabolite in Niemann-Pick type C disease. *Traffic*, **11**, 419–428.
5. Platt, F.M., Boland, B. and van der Spoel, A.C. (2012) The cell biology of disease: lysosomal storage disorders: the cellular impact of lysosomal dysfunction. *J. Cell Biol.*, **199**, 723–734.
6. Rosenbaum, A.I. and Maxfield, F.R. (2011) Niemann-Pick type C disease: molecular mechanisms and potential therapeutic approaches. *J. Neurochem.*, **116**, 789–795.
7. Vance, J.E. and Karten, B. (2014) Niemann-Pick C disease and mobilization of lysosomal cholesterol by cyclodextrin. *J. Lipid Res.*, **55**, 1609–1621.
8. Aqul, A., Liu, B., Ramirez, C.M., Pieper, A.A., Estill, S.J., Burns, D.K., Repa, J.J., Turley, S.D. and Dietschy, J.M. (2011) Unesterified cholesterol accumulation in late endosomes/lysosomes causes neurodegeneration and is prevented by driving cholesterol export from this compartment. *J. Neurosci.*, **31**, 9404–9413.
9. Davidson, C.D., Ali, N.F., Micsenyi, M.C., Stephney, G., Renault, S., Dobrenis, K., Ory, D.S., Vanier, M.T. and Walkley, S.U. (2009) Chronic cyclodextrin treatment of murine Niemann-Pick C disease ameliorates neuronal cholesterol and glycosphingolipid storage and disease progression. *PLoS One*, **4**, e6951.
10. Liu, B., Li, H., Repa, J.J., Turley, S.D. and Dietschy, J.M. (2008) Genetic variations and treatments that affect the lifespan of the NPC1 mouse. *J. Lipid Res.*, **49**, 663–669.
11. Liu, B., Turley, S.D., Burns, D.K., Miller, A.M., Repa, J.J. and Dietschy, J.M. (2009) Reversal of defective lysosomal transport in NPC disease ameliorates liver dysfunction and neurodegeneration in the npc1-/- mouse. *Proc. Natl Acad. Sci. U S A*, **106**, 2377–2382.
12. Maulik, M., Ghoshal, B., Kim, J., Wang, Y., Yang, J., Westaway, D. and Kar, S. (2012) Mutant human APP exacerbates pathology in a mouse model of NPC and its reversal by a beta-cyclodextrin. *Hum. Mol. Genet.*, **21**, 4857–4875.
13. Vite, C.H., Bagel, J.H., Swain, G.P., Prociuk, M., Sikora, T.U., Stein, V.M., O'Donnell, P., Ruane, T., Ward, S., Crooks, A., *et al.* (2015) Intracisternal cyclodextrin prevents cerebellar dysfunction and Purkinje cell death in feline Niemann-Pick type C1 disease. *Sci. Transl. Med.*, **7**, 276ra26.

14. Ward, S., O'Donnell, P., Fernandez, S. and Vite, C.H. (2010) 2-hydroxypropyl-beta-cyclodextrin raises hearing threshold in normal cats and in cats with Niemann-Pick type C disease. *Pediatr. Res.*, **68**, 52–56.
15. Garcia-Robles, A.A., Company-Albir, M.J., Megias-Vericat, J.E., Fernandez-Megia, M.J., Perez-Miralles, F.C., Lopez-Briz, E., Alcala-Vicente, C., Galeano, I., Casanova, B. and Poveda, J.L. (2016) Use of 2 hydroxypropyl-beta-cyclodextrin therapy in two adult Niemann Pick Type C patients. *J. Neurol. Sci.*, **366**, 65–67.
16. Maarup, T.J., Chen, A.H., Porter, F.D., Farhat, N.Y., Ory, D.S., Sidhu, R., Jiang, X. and Dickson, P.I. (2015) Intrathecal 2-hydroxypropyl-beta-cyclodextrin in a single patient with Niemann-Pick C1. *Mol. Genet. Metab.*, **116**, 75–79.
17. Matsuo, M., Shraishi, K., Wada, K., Ishitsuka, Y., Doi, H., Maeda, M., Mizoguchi, T., Eto, J., Mochinaga, S., Arima, H., *et al.* (2014) Effects of intracerebroventricular administration of 2-hydroxypropyl-β-cyclodextrin in a patient with Niemann–Pick Type C disease. *Mol. Genet Metab. Rep.*, **1**, 391–400.
18. Ottinger, E.A., Kao, M.L., Carrillo-Carrasco, N., Yanjanin, N., Shankar, R.K., Janssen, M., Brewster, M., Scott, I., Xu, X., Cradock, J., *et al.* (2014) Collaborative development of 2-hydroxypropyl-beta-cyclodextrin for the treatment of Niemann-Pick type C1 disease. *Curr. Top. Med. Chem.*, **14**, 330–339.
19. Rosenbaum, A.I., Zhang, G., Warren, J.D. and Maxfield, F.R. (2010) Endocytosis of beta-cyclodextrins is responsible for cholesterol reduction in Niemann-Pick type C mutant cells. *Proc. Natl Acad. Sci. U S A*, **107**, 5477–5482.
20. Kwon, H.J., Abi-Mosleh, L., Wang, M.L., Deisenhofer, J., Goldstein, J.L., Brown, M.S. and Infante, R.E. (2009) Structure of N-terminal domain of NPC1 reveals distinct subdomains for binding and transfer of cholesterol. *Cell*, **137**, 1213–1224.
21. Dixit, S.S., Jadot, M., Sohar, I., Sleat, D.E., Stock, A.M. and Lobel, P. (2011) Loss of Niemann-Pick C1 or C2 protein results in similar biochemical changes suggesting that these proteins function in a common lysosomal pathway. *PLoS One*, **6**, e23677.
22. Abi-Mosleh, L., Infante, R.E., Radhakrishnan, A., Goldstein, J.L. and Brown, M.S. (2009) Cyclodextrin overcomes deficient lysosome-to-endoplasmic reticulum transport of cholesterol in Niemann-Pick type C cells. *Proc. Natl Acad. Sci. U S A*, **106**, 19316–19321.
23. Sandhoff, K. (2016) Neuronal sphingolipidoses: Membrane lipids and sphingolipid activator proteins regulate lysosomal sphingolipid catabolism. *Biochimie*, doi: 10.1016/j.biochi.2016.05.004.
24. Malnar, M., Hecimovic, S., Mattsson, N. and Zetterberg, H. (2014) Bidirectional links between Alzheimer's disease and Niemann-Pick type C disease. *Neurobiol. Dis.*,
25. Nixon, R.A. (2004) Niemann-Pick Type C disease and Alzheimer's disease: the APP-endosome connection fattens up. *Am. J. Pathol.*, **164**, 757–761.
26. Love, S., Bridges, L.R. and Case, C.P. (1995) Neurofibrillary tangles in Niemann-Pick disease type C. *Brain*, **118 (Pt 1)**, 119–129.
27. Ohm, T.G., Treiber-Held, S., Distl, R., Glockner, F., Schonheit, B., Tamanai, M. and Meske, V. (2003) Cholesterol and tau protein–findings in Alzheimer's and Niemann Pick C's disease. *Pharmacopsychiatry*, **36 Suppl 2**, S120–S126.
28. Yamazaki, T., Chang, T.Y., Haass, C. and Ihara, Y. (2001) Accumulation and aggregation of amyloid beta-protein in late endosomes of Niemann-pick type C cells. *J. Biol. Chem.*, **276**, 4454–4460.
29. Jin, L.W., Shie, F.S., Maezawa, I., Vincent, I. and Bird, T. (2004) Intracellular accumulation of amyloidogenic fragments of amyloid-beta precursor protein in neurons with Niemann-Pick type C defects is associated with endosomal abnormalities. *Am. J. Pathol.*, **164**, 975–985.
30. Cataldo, A.M., Peterhoff, C.M., Troncoso, J.C., Gomez-Isla, T., Hyman, B.T. and Nixon, R.A. (2000) Endocytic pathway abnormalities precede amyloid beta deposition in sporadic Alzheimer's disease and Down syndrome: differential effects of APOE genotype and presenilin mutations. *Am. J. Pathol.*, **157**, 277–286.
31. Yang, D.S., Stavrides, P., Saito, M., Kumar, A., Rodriguez-Navarro, J.A., Pawlik, M., Huo, C., Walkley, S.U., Cuervo, A.M. and Nixon, R.A. (2014) Defective macroautophagic turnover of brain lipids in the TgCRND8 Alzheimer mouse model: prevention by correcting lysosomal proteolytic deficits. *Brain*, **137**, 3300–3318.
32. Walkley, S.U. and Suzuki, K. (2004) Consequences of NPC1 and NPC2 loss of function in mammalian neurons. *Biochimica Et Biophysica Acta*, **1685**, 48–62.
33. Elrick, M.J., Yu, T., Chung, C. and Lieberman, A.P. (2012) Impaired proteolysis underlies autophagic dysfunction in Niemann-Pick type C disease. *Hum. Mol. Genet.*, **21**, 4876–4887.
34. Lee, J.H., Yu, W.H., Kumar, A., Lee, S., Mohan, P.S., Peterhoff, C.M., Wolf, D.M., Marinez-Vicente, M., Massey, A.G., Sovak, G., *et al.* (2010) Lysosomal proteolysis and autophagy require presenilin 1 and are disrupted by Alzheimer-related PS1 mutations. *Cell*, **141**, 1146–1158.
35. Nixon, R.A., Wegiel, J., Kumar, A., Yu, W.H., Peterhoff, C., Cataldo, A. and Cuervo, A.M. (2005) Extensive involvement of autophagy in Alzheimer disease: an immuno-electron microscopy study. *J. Neuropathol. Exp. Neurol.*, **64**, 113–122.
36. Di Paolo, G. and Kim, T.W. (2011) Linking lipids to Alzheimer's disease: cholesterol and beyond. *Nat. Rev. Neurosci.*, **12**, 284–296.
37. van Echten-Deckert, G. and Walter, J. (2012) Sphingolipids: critical players in Alzheimer's disease. *Prog. Lipid Res.*, **51**, 378–393.
38. Chishti, M.A., Yang, D.S., Janus, C., Phinney, A.L., Horne, P., Pearson, J., Strome, R., Zuker, N., Loukides, J., French, J., *et al.* (2001) Early-onset amyloid deposition and cognitive deficits in transgenic mice expressing a double mutant form of amyloid precursor protein 695. *J. Biol. Chem.*, **276**, 21562–21570.
39. Yang, D.S., Stavrides, P., Mohan, P.S., Kaushik, S., Kumar, A., Ohno, M., Schmidt, S.D., Wesson, D., Bandyopadhyay, U., Jiang, Y., *et al.* (2011) Reversal of autophagy dysfunction in the TgCRND8 mouse model of Alzheimer's disease ameliorates amyloid pathologies and memory deficits. *Brain*, **134**, 258–277.
40. Yao, J., Ho, D., Calingasan, N.Y., Pipalia, N.H., Lin, M.T. and Beal, M.F. (2012) Neuroprotection by cyclodextrin in cell and mouse models of Alzheimer disease. *J. Exp. Med.*, **209**, 2501–2513.
41. Meske, V., Erz, J., Priesnitz, T. and Ohm, T.G. (2014) The autophagic defect in Niemann-Pick disease type C neurons differs from somatic cells and reduces neuronal viability. *Neurobiol. Dis.*, **64**, 88–97.
42. Cheng, J., Ohsaki, Y., Tauchi-Sato, K., Fujita, A. and Fujimoto, T. (2006) Cholesterol depletion induces autophagy. *Biochem. Biophys. Res. Commun.*, **351**, 246–252.

43. Sarkar, S., Carroll, B., Buganim, Y., Maetzel, D., Ng, A.H., Cassady, J.P., Cohen, M.A., Chakraborty, S., Wang, H., Spooner, E., *et al.* (2013) Impaired autophagy in the lipid-storage disorder Niemann-Pick type C1 disease. *Cell Rep.*, **5**, 1302–1315.
44. Tamura, A. and Yui, N. (2016) beta-Cyclodextrin-threaded biocleavable polyrotaxanes ameliorate impaired autophagic flux in Niemann-Pick type C disease. *J. Biol. Chem.*, **290**, 9442–9454.
45. Song, W., Wang, F., Lotfi, P., Sardiello, M. and Segatori, L. (2014) 2-Hydroxypropyl-beta-cyclodextrin promotes transcription factor EB-mediated activation of autophagy: implications for therapy. *J. Biol. Chem.*, **289**, 10211–10222.
46. Sarkar, S. (2013) Regulation of autophagy by mTOR-dependent and mTOR-independent pathways: autophagy dysfunction in neurodegenerative diseases and therapeutic application of autophagy enhancers. *Biochem. Soc. Trans.*, **41**, 1103–1130.
47. Xia, H.G., Zhang, L., Chen, G., Zhang, T., Liu, J., Jin, M., Ma, X., Ma, D. and Yuan, J. (2010) Control of basal autophagy by calpain1 mediated cleavage of ATG5. *Autophagy*, **6**, 61–66.
48. Liang, C. (2010) Negative regulation of autophagy. *Cell Death Differ.*, **17**, 1807–1815.
49. Wei, Y., Pattingre, S., Sinha, S., Bassik, M. and Levine, B. (2008) JNK1-mediated phosphorylation of Bcl-2 regulates starvation-induced autophagy. *Mol. Cell*, **30**, 678–688.
50. Funderburk, S.F., Wang, Q.J. and Yue, Z. (2010) The Beclin 1-VPS34 complex–at the crossroads of autophagy and beyond. *Trends Cell Biol.*, **20**, 355–362.
51. Ishidoh, K. and Kominami, E. (2002) Processing and activation of lysosomal proteinases. *Biol. Chem.*, **383**, 1827–1831.
52. Settembre, C., Di Malta, C., Polito, V.A., Garcia Arencibia, M., Vetrini, F., Erdin, S., Erdin, S.U., Huynh, T., Medina, D., Colella, P., *et al.* (2011) TFEB links autophagy to lysosomal biogenesis. *Science*, **332**, 1429–1433.
53. Martini-Stoica, H., Xu, Y., Ballabio, A. and Zheng, H. (2016) The Autophagy-Lysosomal Pathway in Neurodegeneration: A TFEB Perspective. *Trends Neurosci.*, **39**, 221–234.
54. Sardiello, M., Palmieri, M., di Ronza, A., Medina, D.L., Valenza, M., Gennarino, V.A., Di Malta, C., Donaudy, F., Embrione, V., Polishchuk, R.S., *et al.* (2009) A gene network regulating lysosomal biogenesis and function. *Science*, **325**, 473–477.
55. Macias-Vidal, J., Guerrero-Hernandez, M., Estanyol, J.M., Aguado, C., Knecht, E., Coll, M.J. and Bachs, O. (2016) Identification of lysosomal Npc1-binding proteins: Cathepsin D activity is regulated by NPC1. *Proteomics*, **16**, 150–158.
56. Rigamonti, E., Helin, L., Lestavel, S., Mutka, A.L., Lepore, M., Fontaine, C., Bouhlel, M.A., Bultel, S., Fruchart, J.C., Ikonen, E., *et al.* (2005) Liver X receptor activation controls intracellular cholesterol trafficking and esterification in human macrophages. *Circ. Res.*, **97**, 682–689.
57. Koldamova, R., Fitz, N.F. and Lefterov, I. (2014) ATP-binding cassette transporter A1: from metabolism to neurodegeneration. *Neurobiol. Dis.*, **72 Pt A**, 13–21.
58. Haidar, B., Kiss, R.S., Sarov-Blat, L., Brunet, R., Harder, C., McPherson, R. and Marcel, Y.L. (2006) Cathepsin D, a lysosomal protease, regulates ABCA1-mediated lipid efflux. *J. Biol. Chem.*, **281**, 39971–39981.
59. Oram, J.F. and Heinecke, J.W. (2005) ATP-binding cassette transporter A1: a cell cholesterol exporter that protects against cardiovascular disease. *Physiol. Rev.*, **85**, 1343–1372.
60. Boadu, E. and Francis, G.A. (2006) The role of vesicular transport in ABCA1-dependent lipid efflux and its connection with NPC pathways. *J. Mol. Med. (Berl.)*, **84**, 266–275.
61. Klionsky, D.J., Abdelmohsen, K., Abe, A., Abedin, M.J., Abeliovich, H., Acevedo Arozena, A., Adachi, H., Adams, C.M., Adams, P.D., Adeli, K., *et al.* (2016) Guidelines for the use and interpretation of assays for monitoring autophagy (3rd edition). *Autophagy*, **12**, 1–222.
62. Boland, B., Kumar, A., Lee, S., Platt, F.M., Wegiel, J., Yu, W.H. and Nixon, R.A. (2008) Autophagy induction and autophagosome clearance in neurons: relationship to autophagic pathology in Alzheimer's disease. *J. Neurosci.*, **28**, 6926–6937.
63. Koga, H., Kaushik, S. and Cuervo, A.M. (2010) Altered lipid content inhibits autophagic vesicular fusion. *Faseb J.*, **24**, 3052–3065.
64. Castillo, K., Valenzuela, V., Matus, S., Nassif, M., Onate, M., Fuentealba, Y., Encina, G., Irrazabal, T., Parsons, G., Court, F.A., *et al.* (2013) Measurement of autophagy flux in the nervous system in vivo. *Cell Death Dis.*, **4**, e917.
65. Jankowsky, J.L., Slunt, H.H., Gonzales, V., Savonenko, A.V., Wen, J.C., Jenkins, N.A., Copeland, N.G., Younkin, L.H., Lester, H.A., Younkin, S.G., *et al.* (2005) Persistent amyloidosis following suppression of Abeta production in a transgenic model of Alzheimer disease. *PLoS Med.*, **2**, e355.
66. Nociari, M.M., Lehmann, G.L., Perez Bay, A.E., Radu, R.A., Jiang, Z., Goicochea, S., Schreiner, R., Warren, J.D., Shan, J., Adam de Beaumais, S., *et al.* (2014) Beta cyclodextrins bind, stabilize, and remove lipofuscin bisretinoids from retinal pigment epithelium. *Proc. Natl Acad. Sci. U S A*, **111**, E1402–E1408.
67. Kaushik, S., Massey, A. and Cuervo, A.M. (2006) Lysosome membrane lipid microdomains: novel regulators of chaperone-mediated autophagy. *EMBO J.*, **25**, 3921–3933.
68. Janowski, B.A., Willy, P.J., Devi, T.R., Falck, J.R. and Mangelsdorf, D.J. (1996) An oxysterol signalling pathway mediated by the nuclear receptor LXR alpha. *Nature*, **383**, 728–731.
69. Schroepfer, G.J. Jr. (2000) Oxysterols: modulators of cholesterol metabolism and other processes. *Physiol. Rev.*, **80**, 361–554.
70. Dai, X.Y., Ou, X., Hao, X.R., Cao, D.L., Tang, Y.L., Hu, Y.W., Li, X.X. and Tang, C.K. (2008) The effect of T0901317 on ATP-binding cassette transporter A1 and Niemann-Pick type C1 in apoE-/- mice. *J. Cardiovasc. Pharmacol.*, **51**, 467–475.
71. Zhao, J., Fu, Y., Liu, C.C., Shinohara, M., Nielsen, H.M., Dong, Q., Kanekiyo, T. and Bu, G. (2014) Retinoic acid isomers facilitate apolipoprotein E production and lipidation in astrocytes through the retinoid X receptor/retinoic acid receptor pathway. *J. Biol. Chem.*, **289**, 11282–11292.
72. Wang, M.D., Franklin, V., Sundaram, M., Kiss, R.S., Ho, K., Gallant, M. and Marcel, Y.L. (2007) Differential regulation of ATP binding cassette protein A1 expression and ApoA-I lipidation by Niemann-Pick type C1 in murine hepatocytes and macrophages. *J. Biol. Chem.*, **282**, 22525–22533.
73. Corona, A.W., Kodoma, N., Casali, B.T. and Landreth, G.E. (2016) ABCA1 is Necessary for Bexarotene-Mediated Clearance of Soluble Amyloid Beta from the Hippocampus of APP/PS1 Mice. *J. Neuroimmune Pharmacol.*, **11**, 61–72.
74. Wahrle, S.E., Jiang, H., Parsadanian, M., Kim, J., Li, A., Knoten, A., Jain, S., Hirsch-Reinshagen, V., Wellington, C.L., Bales, K.R., *et al.* (2008) Overexpression of ABCA1 reduces amyloid deposition in the PDAPP mouse model of Alzheimer disease. *J. Clin. Invest.*, **118**, 671–682.

75. Yu, J.T., Tan, L. and Hardy, J. (2014) Apolipoprotein E in Alzheimer's disease: an update. *Annu. Rev. Neurosci.*, **37**, 79–100.
76. Pankiv, S., Clausen, T.H., Lamark, T., Brech, A., Bruun, J.A., Outzen, H., Overvatn, A., Bjorkoy, G. and Johansen, T. (2007) p62/SQSTM1 binds directly to Atg8/LC3 to facilitate degradation of ubiquitinated protein aggregates by autophagy. *J. Biol. Chem.*, **282**, 24131–24145.
77. Komatsu, M. and Ichimura, Y. (2010) Physiological significance of selective degradation of p62 by autophagy. *FEBS Lett.*, **584**, 1374–1378.
78. Fraldi, A., Annunziata, F., Lombardi, A., Kaiser, H.J., Medina, D.L., Spampanato, C., Fedele, A.O., Polishchuk, R., Sorrentino, N.C., Simons, K., *et al.* (2010) Lysosomal fusion and SNARE function are impaired by cholesterol accumulation in lysosomal storage disorders. *EMBO J.*, **29**, 3607–3620.
79. Peake, K.B. and Vance, J.E. (2012) Normalization of cholesterol homeostasis by 2-hydroxypropyl-beta-cyclodextrin in neurons and glia from Niemann-Pick C1 (NPC1)-deficient mice. *J. Biol. Chem.*, **287**, 9290–9298.
80. Neefjes, J. and van der Kant, R. (2014) Stuck in traffic: an emerging theme in diseases of the nervous system. *Trends Neurosci.*, **37**, 66–76.
81. Itakura, E., Kishi-Itakura, C. and Mizushima, N. (2012) The hairpin-type tail-anchored SNARE syntaxin 17 targets to autophagosomes for fusion with endosomes/lysosomes. *Cell*, **151**, 1256–1269.
82. Johnson, C.W., Melia, T.J. and Yamamoto, A. (2012) Modulating macroautophagy: a neuronal perspective. *Future Med. Chem.*, **4**, 1715–1731.
83. Tamboli, I.Y., Hampel, H., Tien, N.T., Tolksdorf, K., Breiden, B., Mathews, P.M., Saftig, P., Sandhoff, K. and Walter, J. (2011) Sphingolipid storage affects autophagic metabolism of the amyloid precursor protein and promotes Abeta generation. *J. Neurosci.*, **31**, 1837–1849.
84. Keilani, S., Lun, Y., Stevens, A.C., Williams, H.N., Sjoberg, E.R., Khanna, R., Valenzano, K.J., Checler, F., Buxbaum, J.D., Yanagisawa, K., *et al.* (2012) Lysosomal dysfunction in a mouse model of Sandhoff disease leads to accumulation of ganglioside-bound amyloid-beta peptide. *J. Neurosci.*, **32**, 5223–5236.
85. Knight, E.M., Williams, H.N., Stevens, A.C., Kim, S.H., Kottwitz, J.C., Morant, A.D., Steele, J.W., Klein, W.L., Yanagisawa, K., Boyd, R.E., *et al.* (2014) Evidence that small molecule enhancement of beta-hexosaminidase activity corrects the behavioral phenotype in Dutch APP mice through reduction of ganglioside-bound Abeta. *Mol. Psychiatry*, **20**, 109–117.
86. Camilleri, P., Haskins, N.J. and Howlett, D.R. (1994) beta-Cyclodextrin interacts with the Alzheimer amyloid beta-A4 peptide. *FEBS Lett.*, **341**, 256–258.
87. Kim, S.I., Yi, J.S. and Ko, Y.G. (2006) Amyloid beta oligomerization is induced by brain lipid rafts. *J. Cell Biochem.*, **99**, 878–889.
88. Yang, D.S., Kumar, A., Stavrides, P., Peterson, J., Peterhoff, C.M., Pawlik, M., Levy, E., Cataldo, A.M. and Nixon, R.A. (2008) Neuronal apoptosis and autophagy cross talk in aging PS/APP mice, a model of Alzheimer's disease. *Am. J. Pathol.*, **173**, 665–681.
89. Rao, M.V., Mohan, P.S., Peterhoff, C.M., Yang, D.S., Schmidt, S.D., Stavrides, P.H., Campbell, J., Chen, Y., Jiang, Y., Paskevich, P.A., *et al.* (2008) Marked calpastatin (CAST) depletion in Alzheimer's disease accelerates cytoskeleton disruption and neurodegeneration: neuroprotection by CAST overexpression. *J. Neurosci.*, **28**, 12241–12254.
90. Micsenyi, M.C., Dobrenis, K., Stephney, G., Pickel, J., Vanier, M.T., Slaugenhaupt, S.A. and Walkley, S.U. (2009) Neuropathology of the Mcoln1(-/-) knockout mouse model of mucolipidosis type IV. *J. Neuropathol. Exp. Neurol.*, **68**, 125–135.
91. Saito, M., Chakraborty, G., Shah, R., Mao, R.F., Kumar, A., Yang, D.S. and Dobrenis, K. (2012) Elevation of GM2 ganglioside during ethanol-induced apoptotic neurodegeneration in the developing mouse brain. *J. Neurochem.*, **121**, 649–661.
92. Mathews, P.M., Jiang, Y., Schmidt, S.D., Grbovic, O.M., Mercken, M. and Nixon, R.A. (2002) Calpain activity regulates the cell surface distribution of amyloid precursor protein. Inhibition of calpains enhances endosomal generation of beta-cleaved C-terminal APP fragments. *J. Biol. Chem.*, **277**, 36415–36424.
93. Yang, D.S., Lee, J.H. and Nixon, R.A. (2009) Monitoring autophagy in Alzheimer's disease and related neurodegenerative diseases. *Methods Enzymol.*, **453**, 111–144.
94. Paxinos, G. and Franklin, K.B.J. (2001) *The mouse brain in streotaxic coordinates*. 2nd Edition ed. Academic Press, London, UK.
95. Schmidt, S.D., Jiang, Y., Nixon, R.A. and Mathews, P.M. (2005) Tissue processing prior to protein analysis and amyloid-beta quantitation. *Methods Mol. Biol.*, **299**, 267–278.
96. Janus, C., Pearson, J., McLaurin, J., Mathews, P.M., Jiang, Y., Schmidt, S.D., Chishti, M.A., Horne, P., Heslin, D., French, J., *et al.* (2000) A beta peptide immunization reduces behavioural impairment and plaques in a model of Alzheimer's disease. *Nature*, **408**, 979–982.
97. Schmidt, S.D., Nixon, R.A. and Mathews, P.M. (2005) ELISA method for measurement of amyloid-beta levels. *Methods Mol. Biol.*, **299**, 279–297.
98. Marks, N. and Berg, M.J. (1987) Rat brain cathepsin L: characterization and differentiation from cathepsin B utilizing opioid peptides. *Arch. Biochem. Biophys.*, **259**, 131–143.
99. Yasuda, Y., Kageyama, T., Akamine, A., Shibata, M., Kominami, E., Uchiyama, Y. and Yamamoto, K. (1999) Characterization of new fluorogenic substrates for the rapid and sensitive assay of cathepsin E and cathepsin D. *J. Biochem.*, **125**, 1137–1143.
100. Eaton, S. (2008) Multiple roles for lipids in the Hedgehog signalling pathway. *Nat. Rev. Mol. Cell Biol.*, **9**, 437–445.
101. Frolov, A., Zielinski, S.E., Crowley, J.R., Dudley-Rucker, N., Schaffer, J.E. and Ory, D.S. (2003) NPC1 and NPC2 regulate cellular cholesterol homeostasis through generation of low density lipoprotein cholesterol-derived oxysterols. *J. Biol. Chem.*, **278**, 25517–25525.